LASER SPECTROSCOPY STUDIES OF $YVO_4:Nd^{3+}$ AND $NdAl_3(BO_3)_4$ CRYSTALS

By

DHIRAJ KUMAR SARDAR

Bachelor of Science
University of Calcutta
Calcutta, India
1968

Master of Science
University of Calcutta
Calcutta, India
1970

Submitted to the Faculty of the Graduate College
of the Oklahoma State University
in partial fulfillment of the requirements
for the Degree of
DOCTOR OF PHILOSOPHY
July, 1980

LASER SPECTROSCOPY STUDIES OF $YVO_4:Nd^{3+}$

AND $NdAl_3(BO_3)_4$ CRYSTALS

Thesis Approved:

Richard C. Powell
Thesis Adviser

Paul Westhaus

J Paul Hawkins

Larry E. Halliburton

W. A. Sibley

Norman N. Durham
Dean of the Graduate College

ACKNOWLEDGMENTS

The author takes the opportunity to express his gratefulness to his thesis adviser, Dr. R. C. Powell, for his help and guidance throughout this work. Special thanks and appreciation are extended to the Graduate Committee members, Dr. P. A. Westhaus, Dr. L. E. Halliburton, and Dr. J. P. Devlin, for their kind cooperation. Finally, the financial support from the Department of Physics, Oklahoma State University, as well as U.S. Army Research Office are gratefully acknowledged by the author.

TABLE OF CONTENTS

LIST OF TABLES

LIST OF FIGURES

CHAPTER I

INTRODUCTION

The study of electronic excitation energy transfer in solids has become an important area of scientific investigations after the development of laser spectroscopic techniques. The rare earth ions have played an important role in the development of modern laser technology and the dynamics of energy transfer is an important process in rare earth doped materials. Understanding the mechanisms of this physical process is, therefore, extremely important and consequently, continued research in this particular field is inevitable.

Solid State Laser Spectroscopic Techniques

Two major laser spectroscopic techniques now being used to investigate laser materials are the following:

1. Time-Resolved Spectroscopy (TRS), and
2. Photoacoustic Spectroscopy (PAS).

In the TRS study, two different types of energy transfer processes can be investigated: (a) host-sensitized energy transfer, and (b) impurity ion-ion interaction processes. The host-sensitized energy transfer is obtained after exciting the host ions or molecules with the fast laser pulses when energy is transferred from host to impurity ions. This type of energy transfer can be studied by monitoring the fluorescence spectra at different times after the laser excitation pulses, and the

results show the time-dependence of energy transfer in the materials under investigation.

The use of high resolution organic dye lasers has enabled us to study the site-selection spectroscopy involving impurity ion-ion interaction process. In this case, it is important to selectively excite ions in specific type of crystal field site with sufficiently narrow band laser and observe energy transfer between ions in different types of crystal sites. This technique is used to examine the changes in the fluorescence spectrum as a function of excitation wavelength and time after the laser pulse.

The PAS technique is a fairly new method to measure the acoustic signals which arise from the radiationless decay of the excited states of rare earth ions in materials exposed to light while in an enclosed cavity. This technique can be used to study the non-radiative decay processes, concentration quenching, and energy transfer processes. Another important aspect of this technique is that the quantum efficiencies of laser materials can be determined.

Properties of Nd Laser Materials

In addition to having an important role in laser technology, the rare earth ions have also many other applications such as phosphors in numerous visual display systems, for example color television, quantum counters, etc. An important type of solid state laser employs the triply charged ion of the rare earth metal neodymium Nd^{3+}, in a variety of host materials.

Yttrium orthovanadate (YVO_4) is one of the many host laser materials developed in recent years. It is important as a host for rare

earth phosphors and lasers, frequency upconverters, infrared polarizers, etc. The general spectroscopic properties of undoped YVO_4 and YVO_4 doped with Eu^{3+}, Er^{3+} and Nd^{3+} have been extensively investigated (18,19) in our laboratory and by others (20-24) in the last few years. The neodymium doped yttrium vanadate crystals have been found to possess some performance characteristics superior to those of standard neodymium doped yttrium aluminum garnet lasers (23). Because of the significant potential of $YVO_4:Nd^{3+}$ as a laser material it has created significant interest in the investigation of the fundamental physical processes underlying its optical properties.

Another example of promising neodymium laser material is neodymium aluminum borate (25) ($Nd\ Al_3[BO_3]_4$). Concentration quenching due to high concentration of Nd^{3+} ions is very much reduced in this material compared to $Y_3Al_5O_{12}$ crystals (25). It is also found (26) that the laser transition cross-section in $Nd\ Al_3(BO_3)_4$ is more than twice as that in $YAG:Nd^{3+}$.

Summary of Thesis

In this work, investigations were made on yttrium orthovanadate crystals doped with 2% and 3% Nd^{3+} ions, and neodymium aluminum borate material to understand the mechanisms which are responsible for the electronic excitation energy transfer in these crystals.

The first part of this work involving host-sensitized energy transfer was done on $YVO_4:Nd^{3+}$ crystals. The absorption spectra of both 2% and 3% neodymium doped samples at room temperature and the fluorescence spectra as function of time after the laser pulse and as function of temperature were taken. The lifetime measurements for both the host

and impurity ions were taken as function of temperature. A theoretical model was proposed to explain the host-sensitized energy transfer based on single step electric dipole-dipole interaction process at low temperatures and multi-step energy migration treated as diffusion process at high temperatures (about 100 K and above).

The second part consisted of the dye laser site-selection spectroscopy of $YVO_4:Nd^{3+}$ and $Nd\ Al_3(BO_3)_4$ crystals. Tunable rhodamine 6 G dye laser was used to selectively excite the ions at different crystal field sites which was demonstrated by the dependences of excitation wavelengths on the structure of fluorescence spectra for both samples. The fluorescence spectra were taken as function of time after the excitation pulse and as function of temperature as well. The lifetimes of the excited states of neodymium ions were also measured at different temperatures. Theoretical models were proposed to explain the energy transfer among neodymium ions based on the multi-step diffusion type energy transfer for $YVO_4:Nd^{3+}$ crystals. The problem of energy transfer by migration among randomly distributed Nd^{3+} impurity ions in YVO_4 was treated (14) with Monte Carlo computer simulation technique and its result was compared with the experimental results obtained from the time-resolved spectroscopic measurements.

In the case of $Nd\ Al_3(BO_3)_4$ sample, the exciton energy transfer rate was found to be time-dependent at both low and high temperatures; and the theoretical model most suitable to interpret the experimental data was one in which the excitation energy undergoes a random walk in one-dimension with phonon-assisted hopping.

The last part of this study was the photoacoustic spectroscopy of neodymium ions doped in yttrium vanadate crystals. C W Argon ion laser

was used to excite the samples which would absorb excitation energy and convert into heat by radiationless deexcitation process. The variation of signal intensity with chopping frequency of incident light was recorded. This particular experimental technique was employed to determine the quantum efficiency of rare earth ions in laser materials and the results were compared with those obtained by other methods.

CHAPTER II

THEORETICAL BACKGROUND

In the study of energy transfer we are interested in two types of ions or atoms. The first one is known as "sensitizer" which absorbs the excitation energy; and the second type is the one which emits the energy and is referred to as the "activator". The process of energy transfer between ions in solids can be grossly divided into the following categories:

1) Single-Step Transfer, and

2) Multistep Diffusion.

Direct transfer from sensitizer to activator ion is known as "single-step" transfer process and its theory was first developed by Förster (1) and Dexter (2). The problem of "multi-step" diffusion among sensitizers was first attacked by Frenkel (3), Förster (1), and Trlifaj (7). The diffusion process can generally be classified as either:

a) Fast Diffusion, or

b) Diffusion Limited.

Single-Step Transfer (Without Diffusion)

In the limit of relatively low sensitizer concentration the exciton can be transferred from a sensitizer to an activator by a single-step process. Sensitizers interact with the activators via exchange or electric multipolar forces. For multipolar interactions the ion-ion

energy transfer rate $\omega_{sa}(R)$ is proportional to an inverse power of their separation (R) and is given by (1)

$$\omega_{sa}(R) = \frac{1}{\tau_s^o}\left(\frac{R_o}{R}\right)^m \equiv \frac{\alpha_{sa}}{R^m} \qquad \text{(II-1)}$$

where τ_s^o is the intrinsic lifetime of sensitizer, R_o is the critical interaction distance, which is defined as the distance between sensitizer and activator at which the energy transfer rate is equal to the intrinsic decay rate, and m is a positive number. This inverse-power rate model (5) covers the following interesting cases:

1) Electric Dipole-Dipole (EDD) interaction for m = 6,

2) Electric Dipole-Quadrupole (EDQ) interactions for m = 8, and

3) Electric quadrupole-quadrupole (EQQ) interaction for m = 10.

In the presence of activators, the number of excited sensitizers varies as (1):

$$n_s(t) = n_s(o)\exp\left[-\frac{t}{\tau_s^o} - \Gamma\left(1-\frac{3}{m}\right)\left(\frac{C_a}{C_o}\right)\left(\frac{t}{\tau_s^o}\right)^{3/m}\right] \qquad \text{(II-2)}$$

where C_a is the activator concentration and C_o is known as the "critical concentration" and defined as

$$C_o = \frac{3}{4\pi R_o^3} \qquad \text{(II-3)}$$

Fast Diffusion

In the case of high sensitizer concentration, where the average sensitizer separation is small compared to sensitizer-activator separa-

tion and when the probability for resonant energy transfer between donors is large, exciton can diffuse through the sensitizers very rapidly. Because of rapid diffusion, the different exciton transfer times for different sensitizer-activator pairs can effectively be averaged out and the exponential decay for excited sensitizer will still remain valid (5).

Diffusion-Limited Transfer

When the activator concentration is fairly high, a large fraction of the sensitizers are within the critical interaction range of activators and then energy migration by diffusion through sensitizers becomes less important. In this situation, energy transfer by diffusion is slow but still comparable with intrinsic decay rate. The excited sensitizer in the neighborhood of activators and far from other sensitizer decay rapidly by direct resonance interaction between sensitizer-activator pair, whereas closer sensitizers first diffuse before they finally get to the activators. This particular situation is named as diffusion-limited energy transfer.

The analytical solution to the diffusion-limited energy transfer process was obtained by Yokota and Tanimoto (4), and the essence of their lengthy and complicated analysis is briefly outlined below.

The general expression for the time evolution of the excited sensitizer density $n_s(\vec{r},t)$ can be obtained by solving the following expression (4):

$$\frac{\partial n_s(\vec{r},t)}{\partial t} = -\frac{1}{\tau_s} n_s(\vec{r},t) + D\nabla^2 n_s(\vec{r},t) - \sum_{i=1}^{N} W_{sa}(\vec{r}-\vec{r}_i) n_s(\vec{r},t) \qquad \text{(III-4)}$$

where τ_s is the sensitizer lifetime, D is the diffusion coefficient,

$W_{sa}(\vec{r}-\vec{r}_i)$ is the interaction strength for a pair of sensitizer at the position $\vec{r}$ and activator at the position $\vec{r}_i$. For EDD interaction the Equation (II-4) can be re-expressed as

$$\frac{\partial n_s}{\partial t} = -\frac{1}{\tau_s} n_s + D\nabla^2 n_s - \sum_i \frac{\alpha_{sa}}{R_i^6} n_s \qquad \text{(II-5)}$$

where $R_i \equiv |\vec{r} - \vec{r}_i|$ is the sensitizer-activator separation. Assumptions of random distribution of activators and uniform distribution of sensitizers were taken (4) in solving the Equation (II-5). The expression for the time-dependent sensitizer concentration can be obtained by integrating the Equation (II-5) over time and averaging over the spatial distribution of randomly distributed activators. Then summing over all the sensitizers the final expression can be obtained (4) as

$$N_s(t) = N_s(0)\, e^{-\frac{t}{\tau_s}} \left\langle e^{t\left(D\nabla^2 - \sum_i \frac{\alpha_{sa}}{R_i^6}\right)} \right\rangle_{av} \qquad \text{(II-6)}$$

where $N_s(t)$ is the total number of excited sensitizers at any time t and $\langle\rangle_{av}$ is the average with respect to activator positions.

Since the assumption of uniform distribution of activators is made, the summation over all sensitizer positions R_i can be replaced by an integral over the crystal volume. Further assumption of low activator concentration is made to evaluate the Equation (II-6) so that each is unaffected by other, and then the decay term which represents the activator averaging can be taken to the N_a^{th} power, where N_a is the total number of activators. Carrying along this line, the rigorous calculations were done by Merkel (8), and applying the [1,2] Pade´ approxi-

mant on the series expansion of the diffusion coefficient in Equation (II-6). The final expression for the total time-dependent sensitizer population is given by (4)

$$N_s(t) = N_s(0) \exp\left[- \frac{t}{\tau_s} - \frac{4}{3} \pi^{3/2} C_a \alpha_{sa}^{1/2} t^{1/2} \left(\frac{1+10.87x+15.50x^2}{1+8.743x}\right)^{3/4} \right] \quad \text{(II-7)}$$

where $x = D \alpha_{sa}^{-1/3} t^{2/3}$. Two limiting cases considered are the following: (1) at short times after the excitation pulse, the EDD interaction between sensitizer and activator becomes the principal contribution to the energy transfer and Equation (II-7) reduces to the well-known expression for energy-transfer rate in the absence of diffusion (1,2); and (2) at long times the diffusion-limited case prevails where the time-independent energy-transfer rate can be expressed as (9):

$$\omega_s = 4\pi D C_a R_T \quad \text{(II-8)}$$

where

$$R_T = 0.676 W_{sa}^{1/4} R_{sa}^{3/2} D^{-1/4} \quad \text{(II-9)}$$

is the trapping radius and R_{sa} is the nearest-neighbor distance between sensitizer-activator pair. The theoretical expression for diffusion coefficient D was obtained by Trlifaj (7) using the approach of a well-known mathematical problem of "random walk" formalism which is found to be equivalent to diffusion mechanism in the limit of many steps in random walk (10) and given by (7)

$$D = 3.4 C_s^{4/3} R_{ss}^6 W_{ss} \quad \text{(II-10)}$$

where, C_s is the sensitizer concentration, R_{ss} is the sensitizer-sensitizer separation, and W_{ss} is interaction strength between a pair of sensitizers. Using Equations (II-9) and (II-10), the final expression for the energy transfer rate is given by

$$\omega_s \approx 21.2\, C_a C_s R_{Nd}^6 W_{ss}^{3/4} W_{sa}^{1/4} \qquad \text{(II-11)}$$

where both R_{ss} and R_{sa} are considered to be equal to the average neodymium ion-ion separation R_{Nd} in the case of our study.

Phonon-Assisted Energy Transfer

The temperature -dependence of energy transfer rate becomes the key in understanding the energy transfer mechanism. In the case of YVO_4:Nd^{3+} samples, it has been found that the activation energy is the same as the crystal field splitting of the $^4F_{3/2}$ metastable state of Nd^{3+} ions in the vanadate host. It is possible that for small energy mismatch situation, the two-phonon-assisted energy transfer process is more effective than the one-phonon-assisted process because the density of states of very low energy phonons is very small. Nonetheless, a transfer process in which one high energy phonon is emitted and another of energy difference by ΔE is absorbed provides quite large density of states; and there are several combinations of possible two-phonon-assisted processes giving rise to different types of temperature dependences for energy transfer rate such as T^3, T^7, and $e^{-\delta/kT}$, where δ is the energy between one of the states involved in transfer process and a real intermediate state reached by phonons involved. In the case of energy transfer study of our interest, the intermediate state was found to be the upper crystal field component of $^4F_{3/2}$ metastable level of Nd^{3+} ions. As the

details of these are very lengthy, only the results (29) will be outlined here.

The two power laws as mentioned above involve nonresonant-phonon-assisted energy transfer within the first excited level. In this case, the one-phonon-electron coupling Hamiltonian is used to the second order, and the result is given for $kT >> |\Delta E|$ as (29)

$$W_{sa}^{Nonres} = \frac{J^2(f-g)}{2\pi^3\rho^2\hbar^7}\left[\sum_s \frac{\alpha_s}{v_s^5}\right]^2 I_2(kT)^3 \qquad \text{(II-12)}$$

where J is the matrix element representing the ion-ion interaction strengths for transfer involving the first excited state and the ground state, f and g are the electron-phonon coupling strengths in the excited and ground states respectively, ρ is the density of the crystal material, v_s is the velocity of sound in crystal, α_s is defined by

$$\alpha_s q^2 \equiv \frac{1}{4}\langle(\vec{e}_{si}\cdot\vec{q}_j + \vec{e}_{sj}\cdot\vec{q}_i)^2\rangle_\Omega \qquad \text{(II-13)}$$

where $\vec{e}_{si}$ and $\vec{e}_{sj}$ are the polarization vectors, $\vec{q}$ is the phonon wave vector, $\langle\rangle_\Omega$ means averaged over solid angle Ω, and I_2 is the integral given by

$$I_2 = \int_0^{\theta_D/T} \frac{x^2\,dx}{(e^x-1)(1-e^{-x})} \qquad \text{(II-14)}$$

which comes in by the use of Debye approximation. Here θ_D is the Debye temperature and $x \equiv \frac{\hbar\omega_{sq}}{kT}$, where ω_{sq} is the phonon frequency with wave vector q and polarization s. For $|\Delta E| << kT << k\,\theta_D$, W_{sa} is approximately

proportional to T^3. The second case of nonresonance two-phonon-assisted energy transfer is obtained by treating the two-phonon-electron coupling Hamiltonian to the first order and the result for $kT >> |\Delta E|$ is

$$W_{sa} = \frac{J^2(f_2-g_2)^2}{4\pi^3\rho^2\hbar^7\Delta E^2}\left[\sum_s \frac{\alpha_s}{v_s^5}\right]^2 I_6(kT)^7 \qquad \text{(II-15)}$$

for $|\Delta E| << kT << k\theta_D$, W_{sa} is proportional to T^7. It should be mentioned that the above results are obtained by assuming qr>1 so that it gives larger average coherence factor defined as (8)

$$\langle h(\vec{k},\vec{r})\rangle_\Omega \approx \frac{k^2r^2}{3} \qquad \text{(II-16)}$$

where

$$h(\vec{k},\vec{r}) = |e^{i\vec{k},\vec{r}} - 1|^2 \qquad \text{(II-17)}$$

is called the coherence factor, and $|\vec{r}|$ is the separation between two ions.

The most important situation for the purpose of our study was the resonant-two-phonon-assisted energy transfer. In this case, there is a closely lying second excited state which can be reached by the phonon energy from the first excited state, and the energy conservation can be obtained by the following three-stage processes illustrated in Figure 1: (1) a phonon of energy $\hbar\omega_{sq}$ is absorbed and the electronic state at Site 1 changes into the upper excited level, (2) a phonon of energy $\hbar\omega_{s'q'}$ is emitted and the electronic state at Site 1 changes back to the first excited level, and (3) EDD interaction occurs. Again, we simply state the results obtained by Orbach et al. (29) for energy transfer rate for the resonance-two-phonon assisted transfer process

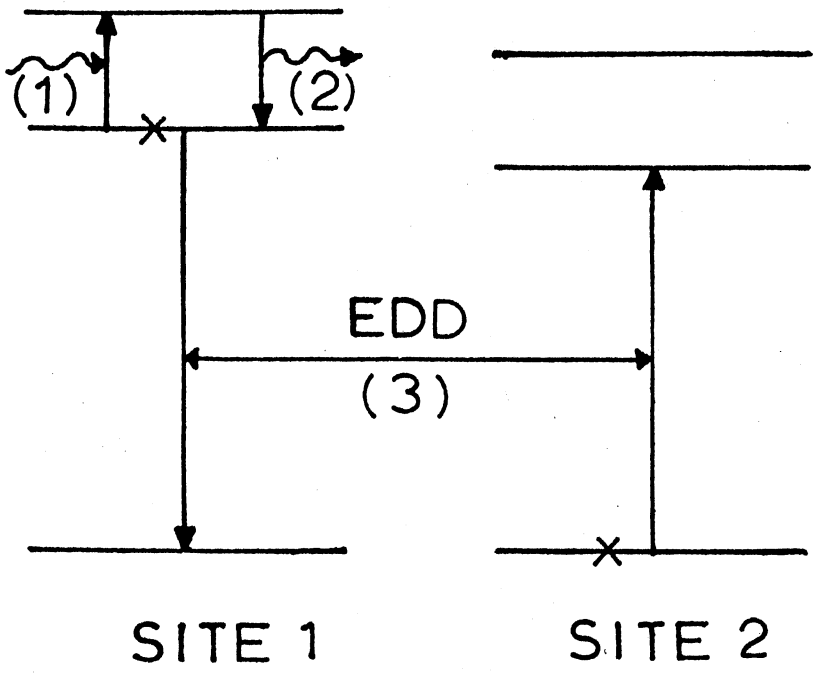

Figure 1. Schematic Diagram for Two Phonon Assisted Energy Transfer

$$W_{res} = \left[J^2 + \frac{2(\Delta E_{12})^2}{(\Delta E_{12})^2 + 8\Gamma_2^2} J_2^2\right] \times \left[\frac{1+e^{\Delta E_{12}/kT}}{(\Delta E_{12})^2}\right] \times \left(\frac{2}{\hbar}\Gamma_2\right) e^{-\delta/kT} \quad \text{(II-18)}$$

where J_2 is the ion-ion interaction strength for transfer involving the second excited state reached by the phonon energy, ΔE_{12} is the energy mismatch, and Γ is the phonon-induced line-width of the second excited state which is the intermediate state. It should be noted that in arriving at the final expression (II-18) the assumptions made are $|\Delta E_{12}| << \delta$ and $\Gamma_2 << kT << \delta \pm \Delta E_{12}$, where the upper and lower sign represents the phonon absorption and emission respectively. It is worth mentioning here that there are several other approaches to the treatment of energy-transfer process involving diffusion among sensitizers as well as direct interaction with activators. The mathematics of energy transfer by hopping among sensitizers and finally from sensitizers to activators will be developed following the Burshtein approach (11-13) below.

Hopping Mechanism in Energy Transfer Among Impurity Ions in Laser Materials (Burshtein Approach)

A crystal is imagined to contain impurity ions randomly distributed in the crystal-lattice, which is pictorially illustrated in Figure 2, where the circles represent the sensitizers and the triangles represent the activators. When a sensitizer is excited with a suitable excitation energy, the sensitizer-excitation transfer can be accomplished by the following ways:

(1) Single-step transfer from sensitizer to activator, and

(2) Multi-step transfer, where exciton may hop from sensitizer

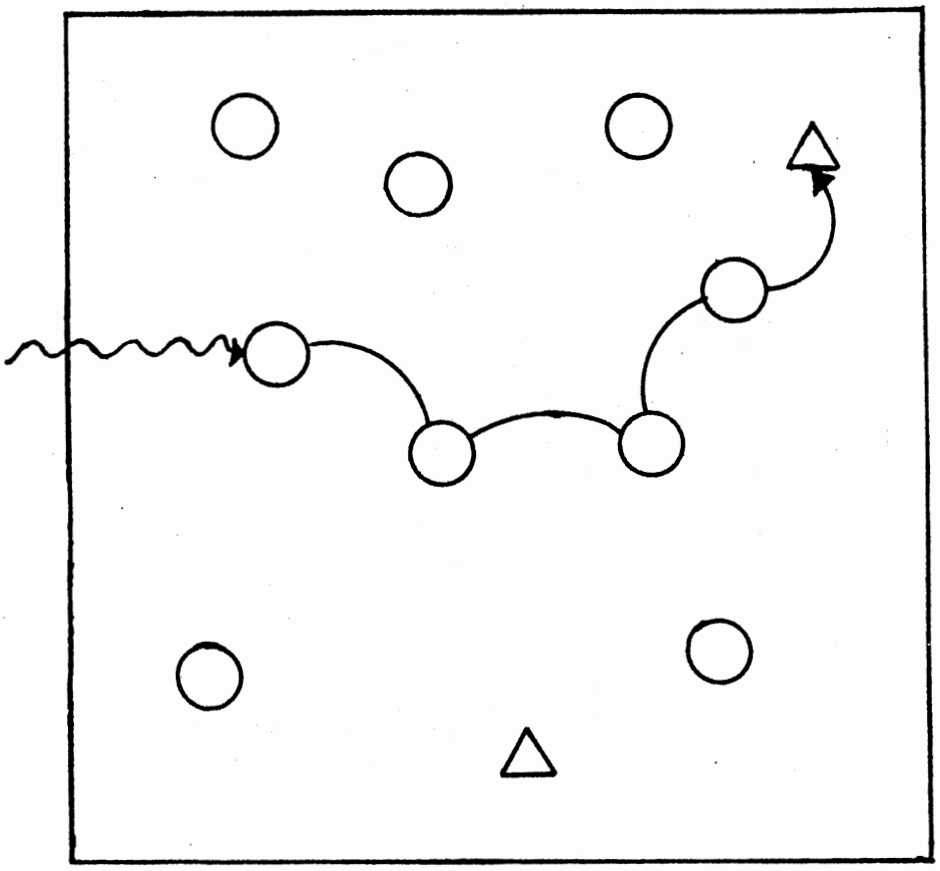

Figure 2. Schematic Diagram for Energy Migration Among Randomly Distributed Activators in a Crystal Lattice

to sensitizer before it finally gets trapped into an activator site. This mechanism is known as hopping process.

Let us first consider the single-step transfer only. The general expression for the time evolution of sensitizer-excitation is given by

$$\frac{\partial n}{\partial t}(\vec{R}_j,t) = -\frac{1}{\tau_s^o} n(\vec{R}_j,t) - \sum_{i=1}^{N_a} \omega(\vec{R}_j-\vec{R}_i) n(\vec{R}_j,t) \qquad \text{(II-19)}$$

where the first term on the right hand side represents decay through radiative or non-radiative or both processes with a decay rate $1/\tau_s^o$, and the second term represents the exciton transfer from a sensitizer at position $\vec{R}_j$ to an activator site at position $\vec{R}_i$ with transfer rate $\omega(\vec{R}_j-\vec{R}_i)$. The sensitizer luminescence decay is usually effected through electric multipolar interaction as already mentioned in the early part of this chapter. For simplicity, we consider only dipole-dipole interaction for which the energy transfer rate is given by (1):

$$\omega_{sa} = \frac{1}{\tau_s^o}\left(\frac{R_o}{R}\right)^6 \equiv \frac{\alpha_{sa}}{R^6} \qquad \text{(II-20)}$$

for sensitizer-activator pair, R being their separation. For sensitizer-sensitizer pair, we can similarly express the energy transfer rate as

$$\omega_{ss} = \frac{\alpha_{ss}}{R^6} \qquad \text{(II-21)}$$

where α_{ss} and α_{sa} are known as interaction constants for the respective pairs. Before solving Equation (II-19) it can be reexpressed simply as

$$\frac{dn_j(t)}{dt} = -\frac{1}{\tau_s^o} n_j(t) - \sum_{i=1}^{N_a} \omega_{sa}(\vec{R})\, n_j(t) \qquad \text{(II-22)}$$

Solution of Equation (II-22) can be written as

$$n_j(t) = n_j(0)\, e^{-t/t_s^o} \prod_{i=1}^{N_a} \exp\left[-t\, \omega_{sa}(\vec{R})\right] \qquad \text{(II-23)}$$

Assuming uniform distribution of ions one can take ensemble average over the whole configuration of sensitizer-activator distribution and obtain

$$\bar{n}(t) = \left\langle \frac{1}{N_s} \sum_{j=1}^{N_s} n_j(t) \right\rangle$$

$$= n(0)\, e^{-t/\tau_s^o} \frac{1}{N_s} \sum_{j=1}^{N_a} \frac{1}{V} \int d^3\vec{R}_j \prod_{i=1}^{N_a} \frac{1}{V} \int d^3\vec{R}\, e^{-t\omega_{sa}(\vec{R})}$$

$$= n(0)\, e^{-t/\tau_s^o} \left[\frac{1}{V} \int d^3\vec{R}\, e^{-t\omega_{sa}(\vec{R})}\right]^{N_a}$$

$$\equiv n(0)\, e^{-t/\tau_s^o} \left[I(t)\right]^{N_a} \qquad \text{(II-24)}$$

where

$$I(t) \equiv \frac{1}{V} \int d^3\vec{R}\, e^{-t\omega_{sa}(\vec{R})} \qquad \text{(II-25)}$$

For dipole-dipole interaction Equation (II-25) can be reexpressed as

$$I(t) = \frac{1}{V} \int_{R_m}^{R_v} 4\pi R^2 dR\, e^{-t/\tau_s^o \left(\frac{R_o}{R}\right)^6} \qquad \text{(II-26)}$$

where R_m is the smallest possible sensitizer-activator spacing and R_v is the radius of the large spherical volume V.

Let us now define the following:

$$x \equiv \frac{t}{\tau_s^o} \left(\frac{R_o}{R}\right)^6$$

$$x_v \equiv \frac{t}{\tau_s^o} \left(\frac{R_o}{R_v}\right)^6 \qquad \text{(II-27)}$$

$$x_m \equiv \frac{t}{\tau_s^o} \left(\frac{R_o}{R_m}\right)^6$$

From the first of Equation (II-27) one can write

$$R^2\, dR = -\frac{1}{6} C^3\, x^{-3/2}\, dx, \quad C \equiv R_o \left(\frac{t}{\tau_s^o}\right)^{1/6} \qquad \text{(II-28)}$$

Using Equations (II-27) and (II-28), one can reexpress Equation (II-26) as

$$I(t) = \frac{1}{2} x_v^{1/2} \int_{x_v}^{x_m} x^{-3/2}\, e^{-x}\, dx$$

or

$$I(t) = \frac{1}{2} x_v \left[\int_o^\infty x^{-3/2}\, e^{-x}\, dx - \int_o^{x_v} x^{-3/2}\, e^{-x}\, dx - \int_{x_m}^\infty x^{-3/2}\, d^{-x}\, dx\right] \qquad \text{(II-29)}$$

Using the Gamma function, $\int_o^\infty x^{n-1}\, e^{-x}\, dx = \Gamma(n)$, for the first term and replacing second and last terms as I_1, and I_2 respectively Equation

(II-29) can be written as

$$I(t) = \frac{1}{2} x_v \left[\Gamma(-\tfrac{1}{2}) - I_1 - I_2 \right] \qquad \text{(II-30)}$$

where

$$I_1 = \int_o^{x_v} x^{-3/2} e^{-x} dx \text{ and}$$

$$I_2 = \int_{x_m}^{\infty} x^{-3/2} e^{-x} dx \qquad \text{(II-31)}$$

I_1 and I_2 can be integrated by parts as

$$I_1 = \int_o^{x_v} x^{-3/2} e^{-x} dx = e^{-x} \frac{x^{-\frac{1}{2}}}{-\frac{1}{2}} \Bigg|_o^{x_v} - \int_o^{x_v} (-e^{-x}) \frac{x^{-\frac{1}{2}}}{-\frac{1}{2}} dx$$

For very small x_v the last term can be neglected and I_1 can be approximated as

$$I_1 \approx -2 e^{-x_v} x_v^{\frac{1}{2}} \qquad \text{(II-31a)}$$

and

$$I_2 = \int_{x_m}^{\infty} x^{-3/2} e^{-x} dx = e^{-x} \frac{x^{-\frac{1}{2}}}{-\frac{1}{2}} \Bigg|_{x_m}^{\infty} - \int_{x_m}^{\infty} (-e^{-x}) \frac{x^{-\frac{1}{2}}}{-\frac{1}{2}} dx$$

For very large x_m the last term can be neglected and one can approximately write as

$$I_2 \approx 2e^{-x_m} x^{-\frac{1}{2}} \qquad \text{(II-31b)}$$

Using the Equations (II-31a) and (II-31b), one can write

$$I(t) = \frac{1}{2} x_v^{\frac{1}{2}} \left[-2\,\Gamma(\tfrac{1}{2}) + 2e^{-x_v} x_v^{-\frac{1}{2}} - 2e^{-x_m} x_m^{-\frac{1}{2}} \right]$$

$$= - x_v^{\frac{1}{2}}\,\Gamma(\tfrac{1}{2}) + e^{-x_v} - x_v^{\frac{1}{2}} e^{-x_m} x_m^{-\frac{1}{2}} \qquad \text{(II-32)}$$

Since x_v is very small, $e^{-x_v} \approx 1 - x_v \approx 1$ and as x_m is very large, the last term of Equation (II-32) can be neglected. Therefore, the Equation (II-32) can be expressed as

$$I(t) \approx 1 - x_v^{\frac{1}{2}}\,\Gamma(\tfrac{1}{2})$$

$$= 1 - \left(\frac{R_o}{R_v}\right)^3 \Gamma(\tfrac{1}{2}) \left(\frac{t_o}{\tau_s}\right)^{\frac{1}{2}}, \qquad \text{[By Eqn. (II-27))}$$

Raising to the power N_a, we get

$$\left[I(t) \right]^{N_a} = \left[1 - \left(\frac{R_o}{R_v}\right)^3 \Gamma(\tfrac{1}{2}) \left(\frac{t_o}{\tau_s}\right)^{\frac{1}{2}} \right]^{N_a} \qquad \text{(II-33)}$$

Activator ion concentration is given by

$$C_a = \frac{N_a}{\frac{4}{3}\pi R_v^3}$$

and from Equation (II-3), critical concentration

$$C_o \approx \frac{3}{4\pi R_o^3} .$$

Taking the ratio of these two concentrations one can obtain

$$\left(\frac{R_o}{R_v}\right)^3 = \left(\frac{C_a}{C_o}\right) \frac{1}{N_a} \qquad \text{(II-34)}$$

Using Equation (II-34), one can reexpress Equation (II-33) as

$$\left[I(t)\right]^{N_a} = \left[1 - \frac{1}{N_a} \left(\frac{C_a}{C_o}\right) \Gamma\left(\frac{1}{2}\right) \left(\frac{t}{\tau}\right)^{\frac{1}{2}}\right]^{N_a} \qquad \text{(II-35)}$$

Since N_a is infinitely large, Equation (II-35) can be approximated as

$$\left[I(t)\right]^{N_a} \approx \exp\left[-\frac{C_a}{C_o} \Gamma\left(\frac{1}{2}\right) \left(\frac{t_o}{\tau_s}\right)^{\frac{1}{2}}\right] \qquad \text{(II-36)}$$

Using Equation (II-36), the Equation (II-24) becomes

$$\bar{n}(t) = n(o) \exp\left[-\frac{t_o}{\tau_s} - \frac{C_a}{C_o} \Gamma\left(\frac{1}{2}\right) \left(\frac{t_o}{\tau_s}\right)^{\frac{1}{2}}\right] \qquad \text{(II-37)}$$

which is the same as Equation (II-2), with m = 2 for dipole-dipole interaction.

Normalizing n(o) to unity, which is the total probability of finding the excited sensitizers at time t = o, when none of the excited sensitizers loses its excitation energy, we can rewrite Equation (II-37) as

$$\bar{n}(t) = \exp\left[-\frac{t_o}{\tau_s} - \sqrt{\Delta t}\right] \qquad \text{(II-38)}$$

where,

$$\Delta \equiv \left(\frac{C_a}{C_o} \sqrt{\frac{\pi}{\tau_s}}\right)^2 \qquad \text{(II-39)}$$

Since $C_o = \frac{3}{4} \pi R_o^3$ and $\alpha_{sa} = \frac{R_o^6}{\tau_s^o}$, Equation (II-39) can be reexpressed as

$$\Delta = \frac{16}{9} \pi^3 C_a^2 \alpha_{sa} \qquad \text{(II-40)}$$

Thus far we have considered only sensitizer-activator transfer due to dipole-dipole interaction. Now, we introduce the exciton migration through hopping from sensitizer to sensitizer before it reaches to some activator site. For simplicity we consider a simple cubic crystal in which there are six nearest neighbors. For dipole-dipole interaction, therefore, the most probable migration rate can approximately be given by

$$\frac{1}{\tau_o} = \frac{\Delta}{6} \qquad \text{(II-41)}$$

In this case,

$$\Delta = \frac{16}{9} \pi^3 C_s^2 \alpha_{ss} \qquad \text{(II-42)}$$

Using Equation (II-42), Equation (II-41) becomes

$$\frac{1}{\tau_o} = \left(\frac{2\pi}{3}\right)^3 C_s^2 \alpha_{ss} \qquad \text{(II-43)}$$

There, τ_o is the average hopping time in the exciton migration process.

In the hopping process, the migration rate varies instantaneously and in a jumpwise fashion (12), and it remains constant between two consecutive jumps. As τ_o is the average hopping time, the probability of

excitation migration from sensitizer to sensitizer can be represented as

$$dW = e^{-t/\tau_o} \frac{dt}{\tau_o} \qquad \text{(II-44)}$$

The reason in considering e^{-t/τ_o} as decay function is for any random physical process the decay probability can never be a sharp one at a particular time nor a constant one all the time. Most probable one for random process is, therefore, chosen to be exponential decay.

It is important now to connect the single step and hopping process discussed above, and obtain the general expression for time development of total sensitizer excitation denoted by $\phi(t)$. Indeed, the connection between $\bar{n}(t)$ and $\phi(t)$ becomes non-local (15) in time, as we have to take the dependence of $\phi(t)$ on $\bar{n}(t)$ during the previous time, say, t' into account. Therefore, the final expression for sensitizer excitation can be given by

$$\phi(t) = \phi(o)\bar{n}(t)e^{-t/\tau_o} + \frac{1}{\tau_o}\int_o^t \phi(t')n(t-t')e^{-\frac{t-t'}{\tau_o}}dt' \qquad \text{(II-45)}$$

This is well known Voltera equation of second kind. Substituting Equation (II-38) in Equation (II-45) and normalizing $\phi(t)$ to unity at time t = o one can arrive at the following expression

$$\phi(t) = e^{-\sqrt{\Delta t} - t/\tau_o} + \frac{1}{\tau_o}\int_o^t e^{-\sqrt{4(t-t')}}\, e^{-\frac{t-t'}{\tau_1}}\phi(t')dt' \qquad \text{(II-46)}$$

Before we solve Equation (II-46), the following substitutions are made

$$\frac{t}{\tau_o} = \xi$$

$$\frac{t'}{\tau_o} = \eta \qquad \text{(II-47)}$$

$$q = \sqrt{\Delta\tau_o}$$

and we can write Equation (II-46) as

$$\phi(\xi) = e^{-q\sqrt{\xi}-\xi} + \int_o^{\xi} e^{-q\sqrt{\xi-\eta}} - (\xi-\eta)\ \phi(\eta)\,d\eta \qquad \text{(II-48)}$$

where q, ξ, and η are dimensionless parameters. Equation (II-48) can now be solved for the following limiting situations:

(1) $q >> 1$, that is, $\alpha_{ss} << \alpha_{sa}$; this is a case of very weak interaction between sensitizer and sensitizer compared to very strong interaction between sensitizer and activator, and

(2) $q << 1$, that is, $\alpha_{ss} >> \alpha_{sa}$; this is a situation of very strong interaction between sensitizer and sensitizer compared to very weak interaction between sensitizer and activator.

Solution for Case (1): $q >> 1$

The Equation (II-48) can be solved for this limiting situation by using the itterative method. Confining ourselves up to first-order approximation we get

$$\phi(\xi) = e^{-q\sqrt{\xi}-\xi} + \int_o^{\xi} e^{-q\sqrt{\xi-\eta}} - (\xi-\eta) \cdot e^{-q\sqrt{\eta}-\eta}\ d\eta$$

$$= e^{-\xi}\left[e^{-q\sqrt{\xi}} + \int_o^{\xi} e^{-q\sqrt{\xi-\eta}} - q\sqrt{\eta}\ d\eta\right]$$

$$\equiv e^{-\xi}\left[e^{-q\sqrt{\xi}} + I(\xi)\right] \qquad \text{(II-49)}$$

where

$$I(\xi) = \int_o^\xi e^{-q\sqrt{\xi-\eta} - q\sqrt{\eta}}\, d\eta$$

$$= \int_o^\xi e^{-q\sqrt{\xi}\,(1-\frac{\eta}{\xi})^{\frac{1}{2}}} \cdot e^{-q\sqrt{\eta}}\, d\eta$$

$$\approx e^{-q\sqrt{\xi}} \int_o^\xi e^{q\eta/2\sqrt{\xi}} \cdot e^{-q\sqrt{\eta}}\, d\eta$$

$$\approx e^{-q\sqrt{\xi}} \int_o^\xi (1 + \frac{q\eta}{2\sqrt{\xi}})\, e^{-q\sqrt{\eta}}\, d\eta$$

$$= e^{-q\sqrt{\xi}}\left[\int_o^\xi e^{-q\sqrt{\eta}}\, d\eta + \frac{q}{2\sqrt{\xi}} \int_o^\xi \eta\, e^{-q\sqrt{\xi}}\, d\eta\right] \qquad \text{(II-50)}$$

Solving the integrals in Equation (II-50) for $q >> 1$, one can get

$$\phi(\xi) = e^{-q\sqrt{\xi} - \xi}\left[1 + \frac{4}{q^2} + \cdots\right] \qquad \text{(II-51)}$$

In this limiting situation ($q >> 1$), Equation (II-51) can be approximated as

$$\phi(\xi) \approx e^{-q\sqrt{\xi} - \xi} \qquad \text{(II-52)}$$

which is similar to Equation (II-38) for single-step electric dipole-dipole transfer between sensitizer and activator only. This is physically unimportant situation in the presence of hopping mechanism.

Solution for Case (2): $q \ll 1$

For this limiting situation, the Equation (II-48) can be solved by using standard method of Laplace transform. Equation (II-48) can be re-expressed as

$$\phi(\xi) = f(\xi) + \int_o^\xi f(\xi-\eta)\ \phi(\eta)\ d\eta$$

Letting $\xi-\eta=\eta'$, we can write

$$\phi(\xi) = f(\xi) + \int_\xi^o f(\eta')\ \phi(\xi-\eta')(-d\eta') \ .$$

Changing $\eta' \to \eta$, we can write

$$\phi(\xi) = f(\xi) + \int_o^\xi f(\eta)\ \phi(\xi-\eta)\ d\eta \qquad \text{(II-53)}$$

By taking Laplace transform of both sides of Equation (II-53), one can get (16)

$$L(p) = F(p) + F(p)L(p)$$

or

$$L(p) = \frac{F(p)}{1-F(p)} \qquad \text{(II-54)}$$

The general solution can, therefore, be obtained by taking the inverse Laplace transform as

$$\phi(\xi) = \frac{1}{2\pi i} \int_{\varepsilon-i\infty}^{\varepsilon+i\infty} \left[\frac{F(p)}{1-F(p)}\right] e^{p\xi}\ dp \qquad \text{(II-55)}$$

where F(p) is the Laplace transform of $e^{-q\sqrt{\xi}-\xi}$, that is,

$$F(p) = \int_o^\infty e^{-p\xi}\, e^{-q\sqrt{\xi}-\xi}\, d\xi$$

$$= \int_o^\infty e^{-\xi(p+1) - q\sqrt{\xi}}\, d\xi \qquad \text{(II-56)}$$

Letting $\sqrt{\xi} = x$, Equation (II-56) can be expressed as

$$F(p) = 2\int_o^\infty x\, e^{-x^2(p+1)-qx}\, dx$$

$$= 2\int_o^\infty x\, e^{-(p+1)\{[x + \frac{q}{2(p+1)}]^2 - [\frac{q}{2(p+1)}]^2\}}\, dx$$

$$= 2\, e^{\frac{q^2}{4(p+1)}} \int_o^\infty x\, e^{-\{x + \frac{q}{2(p+1)}\}^2(p+1)}\, dx$$

Writing $x + \frac{q}{2(p+1)} = u$, we get

$$F(p) = 2\, e^{\frac{q^2}{4(p+1)}} \int_{q/2(p+1)}^\infty [u - \frac{q}{2(p+1)}]\, e^{-u^2(p+1)}\, du$$

$$= 2\, e^{\frac{q^2}{4(p+1)}} [\int_{q/2(p+1)}^\infty u\, e^{-u^2(p+1)}\, du - \frac{q}{2(p+1)} \int_{q/2(p+1)}^\infty$$

$$e^{-u^2(p+1)}\, du]$$

$$\equiv 2\, e^{\frac{q^2}{4(p+1)}}\, [I' - I''] \qquad \text{(II-57)}$$

where

$$I' = \int_{q/2(p+1)}^\infty u\, e^{-u^2(p+1)}\, du \qquad \text{(II-58)}$$

and

$$I'' = \frac{q}{2(p+1)} \int_{q/2(p+1)}^{\infty} e^{-u^2(p+1)}\, du$$

I' and I" are integrals which are simple enough to solve and the results are

$$I' = \frac{1}{2(p+1)}\, e^{-q^2/4(p+1)} \tag{II-59}$$

and

$$I'' = \frac{q\sqrt{\pi}}{4(p+1)^{3/2}} \left[1 - \operatorname{erf}\left(\frac{q}{2\sqrt{p+1}}\right)\right]$$

Substituting Equation (II-59) in Equation (II-57), we get

$$F(p) = 2\, e^{\frac{q^2}{4(p+1)}} \left[\frac{1}{2(p+1)}\, e^{-\frac{q^2}{4(p+1)}} - \frac{q\sqrt{\pi}}{4(p+1)^{3/2}} \left\{1 - \operatorname{erf}\left(\frac{q}{2\sqrt{p+1}}\right)\right\}\right]$$

$$= \frac{1}{p+1}\left[1 - \frac{1}{2}\sqrt{\frac{\pi q^2}{p+1}}\; e^{\frac{q^2}{4(p+1)}} \left\{1 - \operatorname{erf}\left(\frac{q}{2\sqrt{p+1}}\right)\right\}\right] \tag{II-60}$$

For the limiting situation $q \ll 1$, we can expand the error-function as

$$\operatorname{erf}\left(\frac{q}{2\sqrt{p+1}}\right) = \frac{2}{\sqrt{\pi}} \cdot \frac{q}{2\sqrt{p+1}} \left[1 - \frac{q^2}{4(p+1)} \cdot \frac{1}{3} + \frac{q^4}{16(p+1)^2} \cdot \frac{1}{10} - \cdots\right]$$

$$= \frac{q}{\sqrt{\pi}\,\sqrt{p+1}} - \frac{q^3}{12(p+1)^{3/2}} + \cdots \tag{II-61}$$

Substituting Equation (II-61) into Equation (II-60), one can obtain

$$F(p) = \frac{1}{p+1}\left\{1 - \left(\frac{q}{2}\sqrt{\frac{\pi}{p+1}} + \frac{q^3\sqrt{\pi}}{8(p+1)^{3/2}} + \cdots\right)\left(1 - \frac{q}{\sqrt{\pi}\sqrt{p+1}}\right.\right.$$

$$\left.\left. + \frac{q^2}{12(p+1)^{3/2}} + \cdots\right)\right\}$$

Keeping up to third power of q, we get

$$F(p) = \frac{1}{p+1} - \frac{q\sqrt{\pi}}{2(p+1)^{3/2}} + \frac{q^2}{2(p+1)^2} - \frac{q^3\sqrt{\pi}}{8(p+1)^{5/2}} + \cdots \qquad \text{(II-62)}$$

Now,

$$1 - F(p) = 1 - \frac{1}{p+1} + \frac{q\sqrt{\pi}}{2(p+1)^{3/2}} - \frac{q^2}{2(p+1)^2} + \cdots$$

$$\approx 1 - \frac{1}{p+1} \quad (\because q << 1)$$

Hence,

$$\frac{F(b)}{1-F(b)} = \frac{\frac{1}{p+1} - \frac{q\sqrt{\pi}}{2(p+1)^{3/2}} + \frac{q^2}{2(p+1)^2} - \cdots}{\frac{p}{p+1}} \approx \frac{1}{p} - \frac{q\sqrt{\pi}}{2}\left[\frac{1}{p(p+1)^{\frac{1}{2}}}\right]$$

$$+ \frac{q^2}{2}\left[\frac{1}{p(p+1)}\right] \qquad \text{(II-63)}$$

Using standard table of Laplace transfer for the terms in Equation (II-63) and substituting for the general expression (II-55), one can arrive at the following result:

$$\phi(\xi) = 1 - \left(\frac{q\sqrt{\pi}}{2} - \frac{q^2}{2} + \cdots\right)\xi \qquad \text{(II-64)}$$

In our limiting situation Equation (II-64) can be expressed as

$$\phi(\xi) = e^{-(\frac{q\sqrt{\pi}}{2} - \frac{q^2}{2} + \cdots)\xi}$$

Since $\xi = \frac{t}{\tau_o}$, we can rewrite the above equation as

$$\phi(t) = e^{-(\frac{q}{2}\sqrt{\pi} - \frac{q^2}{2} + \cdots)\frac{t}{\tau_o}} \equiv e^{-\omega_{(hop)} t} \qquad \text{(II-65)}$$

where

$$\omega_{(hop)} = \frac{1}{\tau_o}(\frac{q\sqrt{\pi}}{2} - \frac{q^2}{2} + \cdots) \qquad \text{(II-66)}$$

Equation (II-65) indicates an exponential decay. The principal term in it for the particular limiting situation is the following:

$$\omega_{(hop)} = \frac{q\sqrt{\pi}}{2\tau_o} = \sqrt{\frac{\pi}{2}}\sqrt{\frac{\Delta}{\tau_o}} \qquad \text{(II-67)}$$

Substituting Δ from Equation (II-40) and τ_o from Equation (II-43), the Equation (II-67) becomes

$$\omega_{(hop)} = \frac{2\pi^2}{3}(\frac{2\pi}{3})^{3/2} C_a C_s (\alpha_{sa}\alpha_{ss})^{1/2}$$

$$\simeq 19.9\, C_a C_s (\alpha_{sa}\alpha_{ss})^{\frac{1}{2}} \qquad \text{(II-68)}$$

The difference between the exciton decay rate given by Equation (II-68) by hopping and the exciton transfer rate by diffusion-limited process expressed in Equation (II-11) lies in different dependences in the interaction constants, but they have same dependence in the sensitizer and activator concentrations.

The theoretical development of hopping mechanism in exciton migration in light of Burshtein approach is quite straightforward. But it

involves many approximations, the most controversial one of those is assuming a constant average hopping time. Especially, in lightly doped samples this assumption is, perhaps, very unrealistic one. Recently, a Monte-Carlo computer simulation technique has been employed (14) to treat the above mentioned problem. The essence of that technique is given here. A set of finite number of excitons are generated by computer and allowed to hop. The numbers are then weighted by a Hertzian distribution which is the law of distribution of nearest-neighbors in a three-dimensional random array of sites. The common dipole-dipole interaction has been chosen for their interaction strength. At every step in the hopping process, one of the excitons is chosen as the hopping time for the next hop. After each hop, the site is designated as either a sensitizer or an activator, and each exciton is allowed to hop until either it gets trapped at the activator site or the hopping time is longer than the time of interest in the experiment which was arbitrarily chosen in our study to be 10 times the sensitizer lifetime. Finally, total number of excitons alive at each time after the excitation pulse, is determined. The results obtained from TRS measurements are finally compared with the predictions of this computer simulation technique.

CHAPTER III

SAMPLES AND APPARATUS

A brief description of the samples investigated and the experimental techniques as well as equipments employed in this study will be provided here in this chapter. Two types of samples studied were yttrium vanadate doped with neodymium impurity ions and neodymium aluminum borate. As was already mentioned in Chapter I, two major experimental techniques used in this investigation were time-resolved and photoacoustic spectroscopy.

Samples

Two single crystals of YVO_4 doped with 2.55×10^{22} cm^{-3} and 3.82×10^{20} cm^{-3}, Nd^{3+} ions; and small single crystal pieces of $Nd\ Al_3(BO_3)_4$ were investigated. The thicknesses of the $YVO_4:Nd^{3+}$ single crystals were 0.155 cm and 0.239 cm respectively. The crystallographic structure (27) of pure YVO_4 is that of zircon and there are four molecules per unit cell with dimensions of a = 7.123 Å and c = 6.291 Å. The space group of YVO_4 crystal structure is D_{4h}^9. The vanadium ion is tetrahedrally coordinated with oxygen ion to form vanadate VO_4^{3-} molecular ions with T_d symmetry, and the vanadium-oxygen spacing is of 1.721Å. These VO_4^{3-} molecular ions as well as Y^{3+} ions, however, belong to D_{2d} symmetry sites in the YVO_4 crystal.

The crystal structure (25) of $Nd\ Al_3(BO_3)_4$ is rhombohedral with space group R32 and unit cell dimensions of a = 9.3416Å and c = 7.3066Å.

The structure of this crystal consists of two sets of isolated $(BO_3)^{3-}$ triangles. The Nd^{3+} and Al^{3+} ions form trigonal prisms and octahedra of oxygen respectively. The Nd^{3+} ions forming isolated and trigonal prisms with oxygen are connected alternatively by B^{3+} and Al^{3+} ions. The Al^{3+} ions forming octahedra with oxygen share edges to form helices along the c-axis and are connected with $(BO_3)^{3-}$ triangles. The crystal structure of $Nd\ Al_3(BO_3)_4$ is, however, fairly complex with significant lack of inversion symmetry (25). In these crystals the high concentration ($5.43 \times 10^{21}\ cm^{-3}$) of Nd^{3+} ions can be present without strong concentration quenching due to the isolation of Nd polyhedra. The strong odd-parity crystal field admixture of the f and d electrons results in a short radiative lifetime and the large transition cross section (26) of Nd^{3+} ions in the laser materials.

Experimental Techniques and Apparatus

Laser time-resolved spectroscopy is a technique in which time evolution of a fluorescence spectrum is obtained after the laser excitation. The schematic diagram of the experimental set-up of the TRS technique is shown in Figure 3. For host-sensitized energy transfer studies a pulsed nitrogen laser was used as excitation source of the sample under investigation. The nitrogen laser is a National Research Group (NRG) spark gap triggered laser which gives off a pulse of 8 ns duration and about 0.35 MW peak power at 3371Å. The repetition rate of 30 Hz was used throughout the investigation and the half-width of the laser line is less than 0.4Å.

For site-selection spectroscopic investigations a tunable dye laser containing rhodamine 6G and pumped by the nitrogen laser was used to

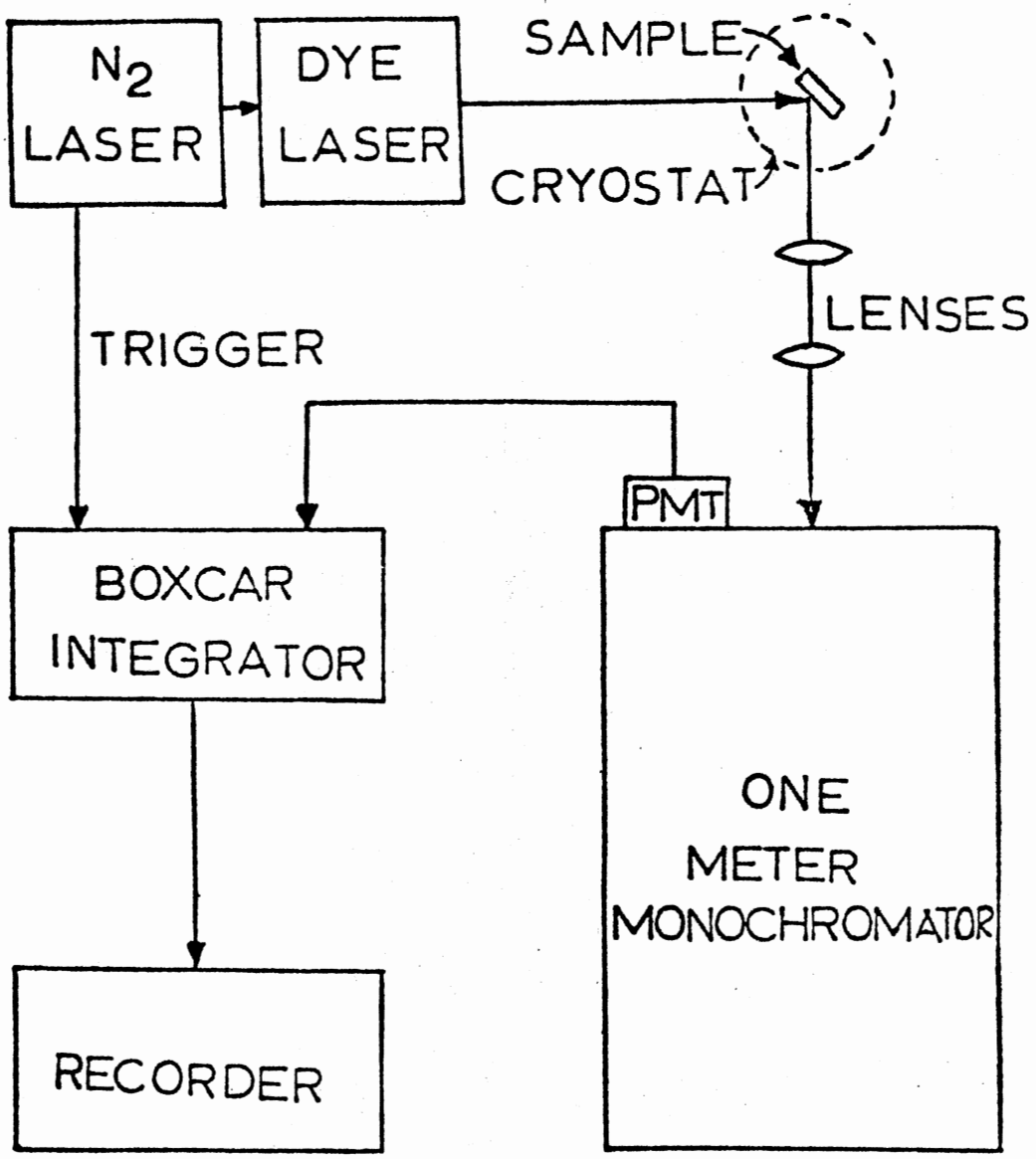

Figure 3. Time Resolved Spectroscopy Apparatus

selectively excite the neodymium ions in the specific crystal field site. The nitrogen laser output is focused into the dye cell with the help of a set of convex and cylindrical lenses. Focusing is performed only when the dye is flowing inside the cell to avoid the damage from heat. The fluorescence from the dye comes along the axis of the resonant cavity which is formed by a partially silver coated mirror and a grating used as a rear reflecting mirror. A beam expanding telescope in the cavity is used to increase the coverage of grating; and the fine adjustment of the telescope helps select very narrow wavelength reflected back through the cavity. As the organic dye can be used to lase over a wide wavelength range, the combination of grating and telescope is used to obtain very narrow tunable laser line. Of course, the fine and critical adjustments of lenses and dye cell are extremely important to improve the lasing quality. The duration of the laser pulse was less than 10 ns and the half-width of the dye laser pulse was less than 0.4Å.

The fluorescence signals were collected at a right angle with the laser excitation beam direction and focused onto the entrance of slit of a spex, one meter Czerney-Turner Spectromator Model 1704. For the purpose of our studies the spectromator was equipped with a grating which is blazed at 1 micron and has 600 grooves per mm. The slit-width can be varied depending on the particular situation of investigation. The signal was detected by a thermoelectrically cooled RCA C31034 phototube with a 20 megaohm load resistor which was operated at -1900 V DC. The output of the phototube was processed by a Princeton Applied Research (PAR) Corp. Model 162 boxcar averager with processor modules to form a gated signal recovery system. The averager is triggered directly from the nitrogen laser in both laser systems. A variable load resistor used

in parallel with the input impedance of the box car was used to make adjustment of time constant of the input circuit so that undistorted signals could be obtained. The box car contains a time aperture which can be set from 0.10 μs to 50 ms after a triggering signal, and the box car accepts the input signal only during a selected time aperture which may be scanned to obtain lifetime data by setting the spectromator at a fixed wavelength, whereas the time aperture could be set a constant time after the laser pulse to obtain the fluorescence spectrum by scanning the spectromator with suitable scan speed. The signals were finally recorded on x-y recorder for lifetime data and on strip chart recorder for fluorescence spectra.

For low temperature measurements the samples were mounted on the cold finger of a closed cycle helium cryogenic refrigerator of Air Products and Chemicals Displex Model CS-202. By balancing the heat from a small electric heater circuit installed on the cold finger against the absorption of heat by the refrigerator, sample temperature can be varied from 8 K up to room temperature. The temperature of the sample is measured by a thermocouple made of Gold (0.07% iron) versus chromel.

Absorption and Excitation Measurements

The optical absorption spectra were taken by a Cary Model 14 Spectrometer at room temperature; using the tungsten-halogen light source in the visible region. Because of large absorption coefficient of YVO_4 in the ultraviolet region, absorption measurements were not made in this region.

The excitation spectrum of Nd $Al_3(BO_3)_4$ was taken using the apparatus shown in Figure 4. The light from a 150 W xenon lamp was focused

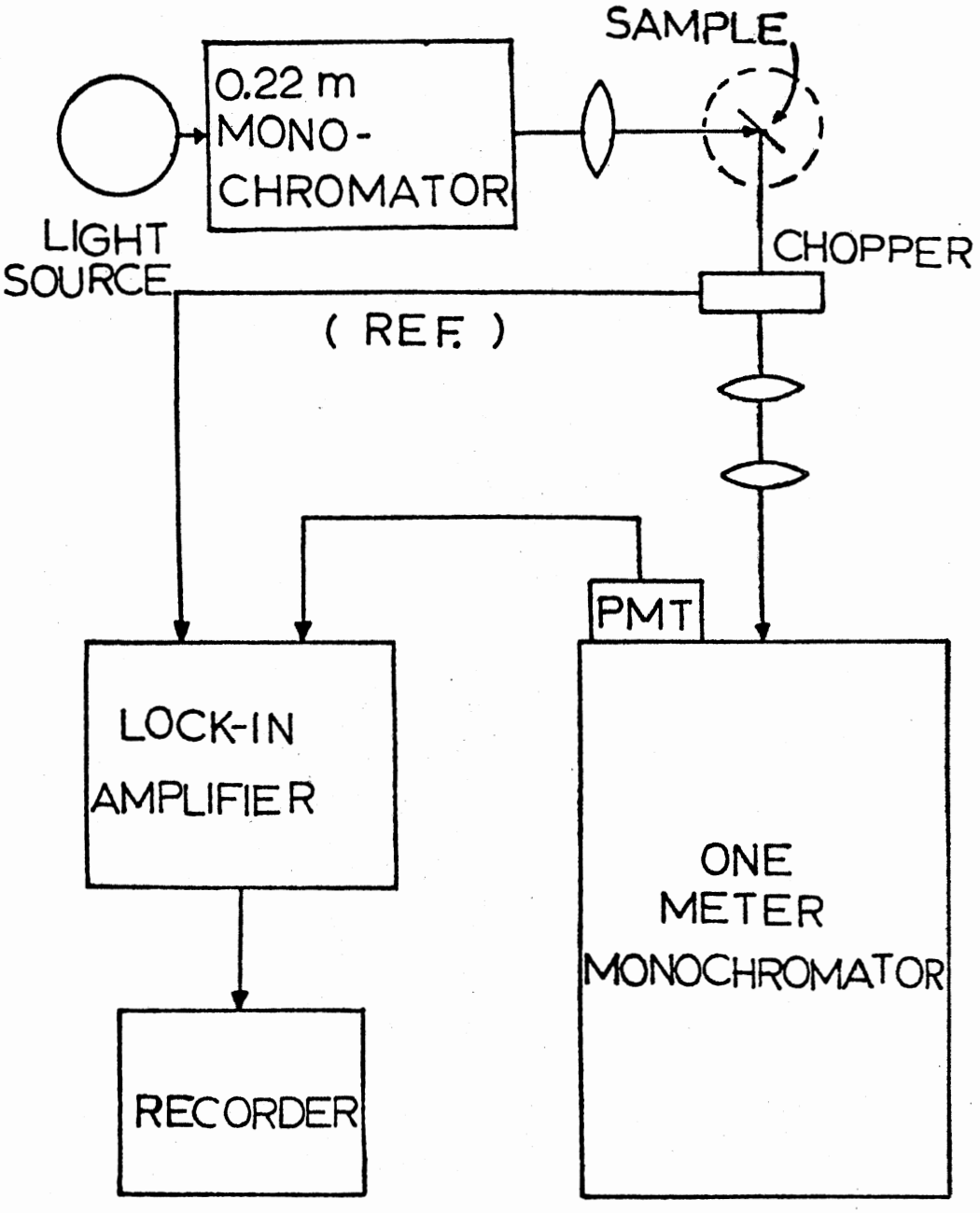

Figure 4. Block Diagram of Excitation Apparatus

onto the entrance slit of a Spex Model 1670 minimate motor driven monochromator and the output of the scanning monochromator was focused on the sample. The fluorescence signal collected at 90^{o} with the excitation light path was chopped by a PAR Model 125 mechanical chopper at a frequency of 1000 Hz. The chopped fluorescence signals were analyzed by one meter Czerny-Turner Spectromator and detected by cooled photomultiplier tube as described before.

The output of the photomultiplier tube was processed by a PAR Model 128 lock-in amplifier and the reference was taken from the chopper. The excitation spectrum was taken by keeping the wavelength fixed on the one meter Czerney-Turner spectrometer and scanning the wavelength of the excitation light by the minimate monochromator. Finally, the output was recorded on a strip chart recorder.

Photoacoustic Spectroscopy

Photoacoustic spectroscopy copy (PAS), is a fairly new technique and is employed to investigate the radiationless relaxation processes of ions in laser materials. The PAS studies were performed on both 2% and 3% Nd^{3+} doped YVO_4 crystals. The experimental set up used for these investigations is depicted in Figure 5. The individual line of an argon ion laser were used as the excitation source; and the laser power was continuously monitored and stabilized at a level of 0.15 W. The incident light was chopped at different frequencies ranging from 110 to 2000 Hz by mechanical light chopper and focused onto the sample which was placed on a quartz exit window of the PAS sample cell made of aluminum chamber with a quartz input window. A microphone was mounted at the side of chamber and an aluminum foil baffle was used to prevent scattered

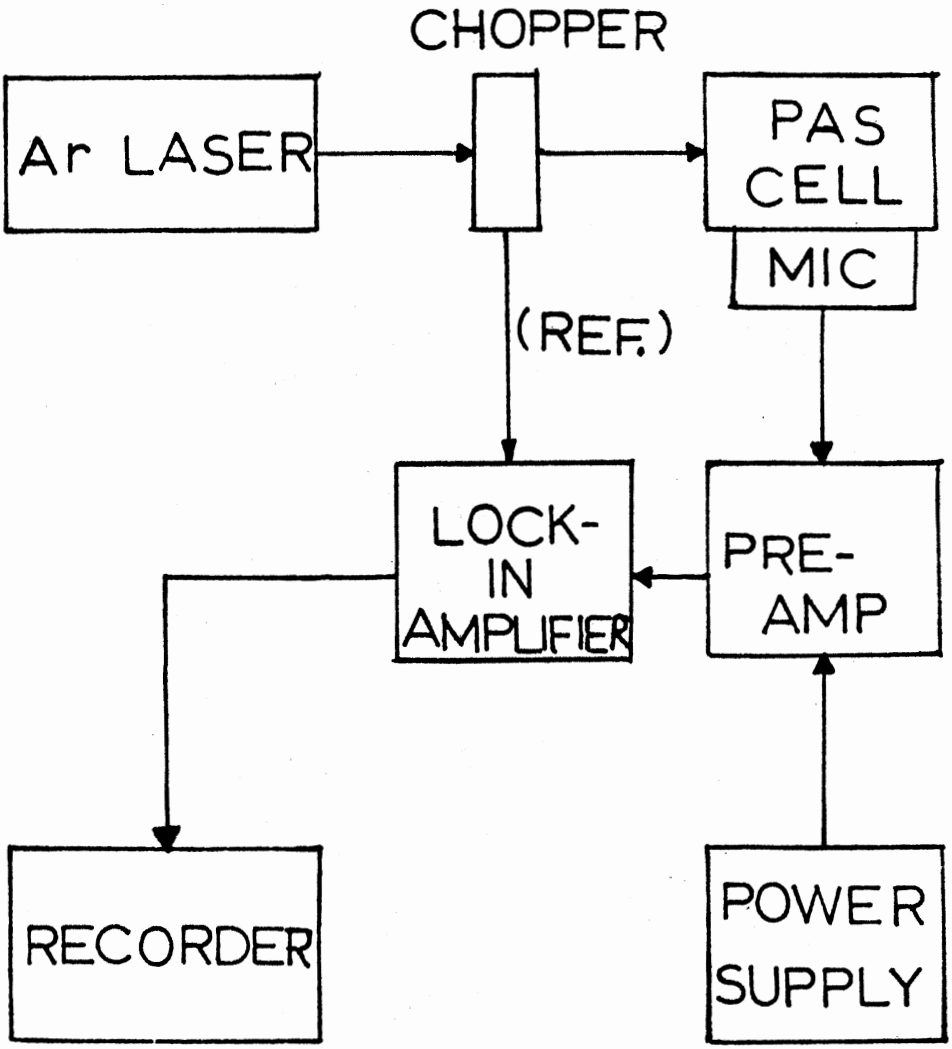

Figure 5. Photoacoustic Spectroscopy Apparatus

light from reaching the microphone which collects the PA signals. The signal from the microphone was amplified using a PAR Model 115 wide-band preamplifier and processed by a PAR Model 128 lock-in amplifier which received its reference signal from the light chopper. The signal was finally read out on a digital voltmeter after adjusting the lock-in phase to maximize the signal.

The samples investigated by PAS technique were 2% and 3% Nd^{3+} doped YVO_4 single crystals with polished faces. Two types of measurements were done:

1) measurement of PA signal intensity versus chopping frequency and,

2) determinaton of quantum efficiencies.

CHAPTER IV

HOST SENSITIZED ENERGY TRANSFER IN $YVO_4:Nd^{3+}$ CRYSTALS

Experimental Results

The yttrium vanadate host crystals were excited with the pulsed nitrogen laser at 3371Å and energy transfer from host VO_4^{3-} to Nd^{3+} impurity ions was studied by monitoring the fluorescence spectra at different times after the laser pulse and by measuring the fluorescence lifetimes for the host and Nd^{3+} emissions as a function of temperature.

The typical room temperature absorption spectrum of a 1.55 mm thick $YVO_4:Nd^{3+}$ sample with Nd concentration of 2.55×10^{22} cm^{-3} is shown in Figure 6. The fluorescence lifetimes are shown as a function of temperature in Figure 7 and listed in Table I for the 3% sample. The lifetime of the $^4F_{3/2}$ metastable state of Nd^{3+} shows very little dependence on temperature while the host fluorescence lifetime shows strong temperature dependence. The host fluorescence lifetimes of the doped and undoped (19) samples show similar temperature dependences except that the magnitudes of lifetimes of doped sample are smaller than those of the undoped ones due to energy transfer. The rate of energy transfer ω can be derived from this lifetime quenching as

$$\omega = \frac{1}{\tau_H} - \frac{1}{\tau_H^o} \qquad \text{(IV-1)}$$

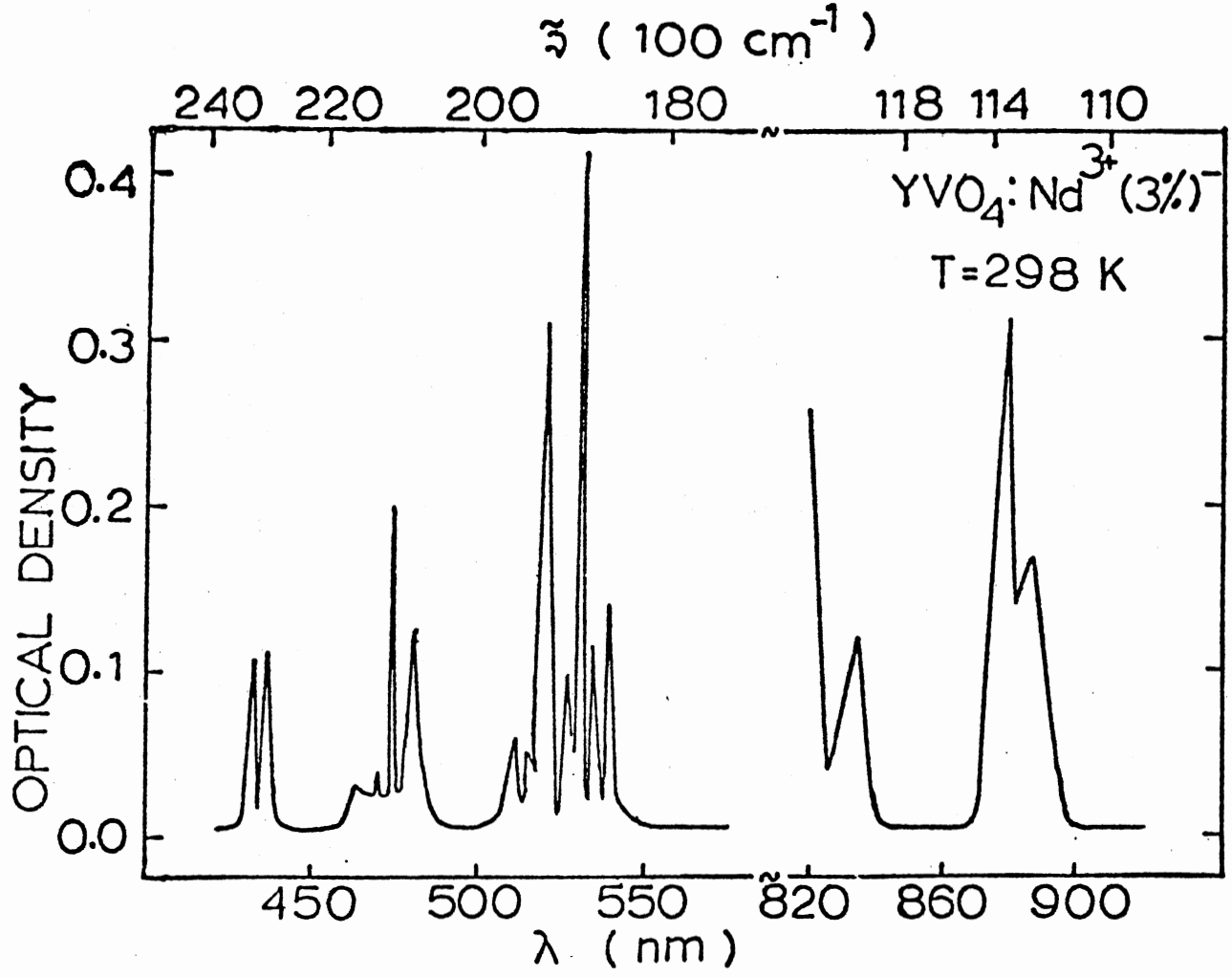

Figure 6. Room Temperature Absorption Spectrum of $YVO_4:Nd^{3+}$ (3%); Sample Thickness is 1.55 mm

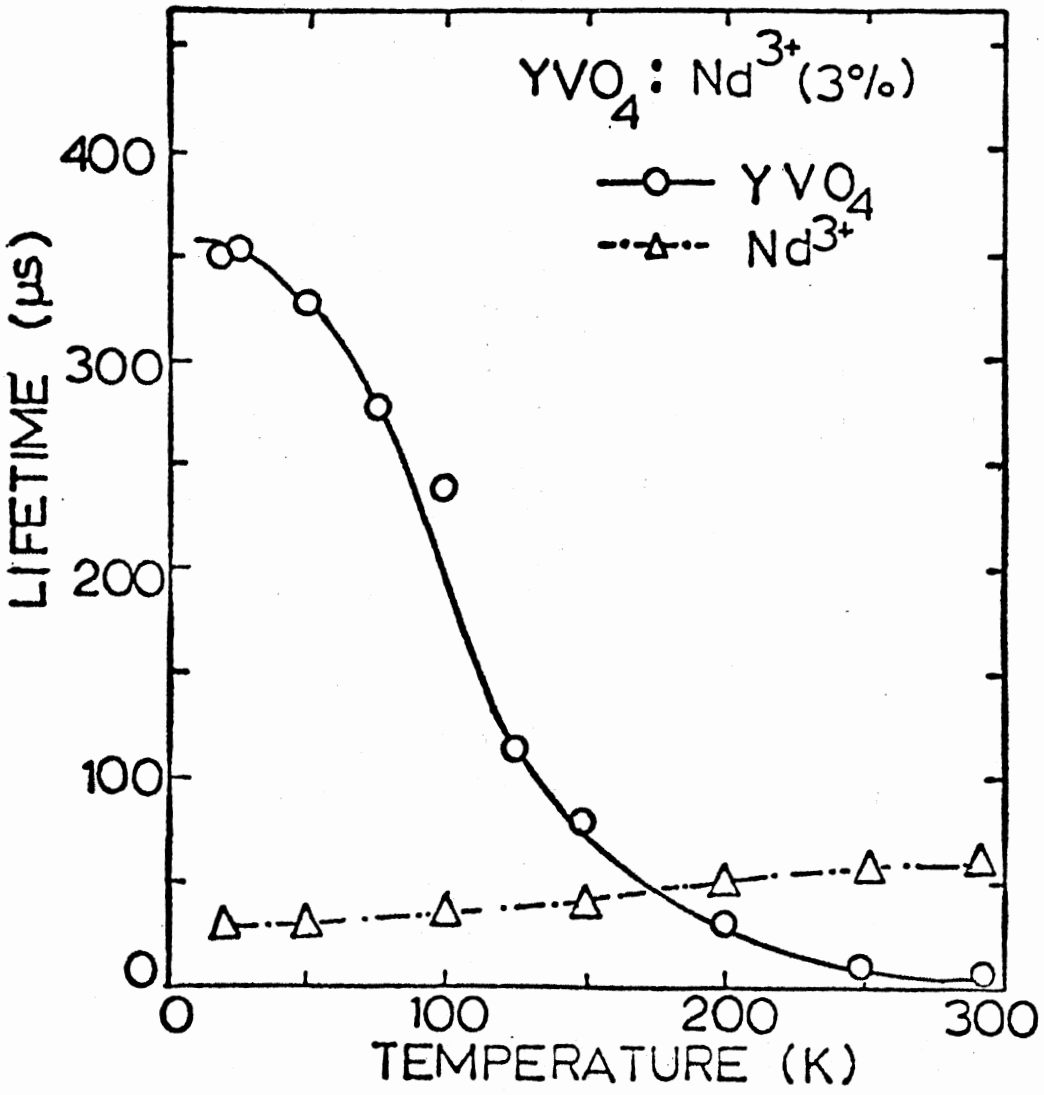

Figure 7. Temperature Dependences of $YVO_4:Nd^{3+}$ After Excitation With a Pulsed N_2 Laser

TABLE I

FLUORESCENCE LIFETIMES FOR $YVO_4:Nd^{3+}$ (3%) SYSTEM AT DIFFERENT TEMPERATURES

T(K)	Host:YVO_4 Lifetime (μs)	Impurity Nd^{3+} Lifetime (μs)
8	350	26
19	352	29
25	352	29
50	328	37
75	280	35
100	240	40
125	1105	41
150	80	51
200	30	54
250	9	55
294	7	55

where τ_H^o and τ_H are the host fluorescence lifetimes in the undoped and doped samples, respectively. The temperature dependence of the energy transfer rate is shown in Figure 8 and tabulated in Table II. The figure shows that the energy transfer rate is approximately constant at low temperatures and dincreases exponentially at temperatures above about 75K. The activation energy for this increase in transfer rate was found to be about 250 cm^{-1}.

Figure 9 shows the fluorescence spectra of $YVO_4:Nd^{3+}$ taken at short and long times after the laser pulse and observed at 11K, where the host fluorescence intensity is seen to decrease with time after the laser pulse while the neodymium fluorescence intensity increases. This indicates that energy transfer is taking place between the excited vanadate molecular ions and the neodymium ions.

The results of TRS investigations at 11K and 100K are shown in Figure 10 and tabulated in Table III.

Interpretation of Results

The TRS data was interpreted using the phenomenological model shown in Figure 11, in which n_H and n_T represent the concentrations of excited states of the host and impurity ions respectively, while B_H and B_T are their fluorescence decay rates. W represents the rate of creation of host excited states and ω is the rate of energy transfer between host and impurity ions (traps). The rate equations for the excited state populations are

$$dn_H/dt = W - B_H n_H - \omega n_H \qquad \text{(IV-2)}$$

$$dn_T/dt = \omega n_H - B_T n_T \qquad \text{(IV-3)}$$

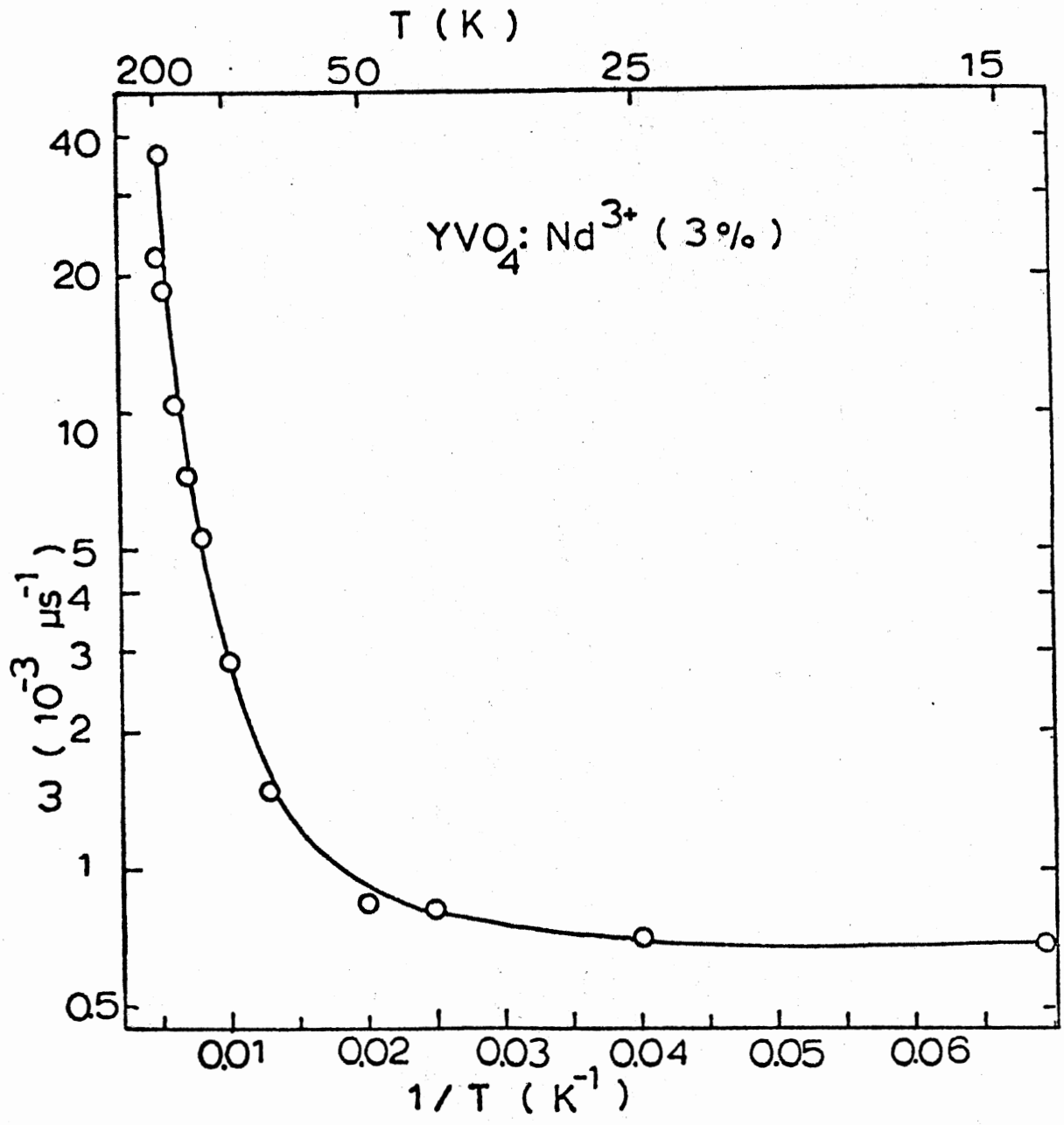

Figure 8. Temperature Dependence of the Host-Sensitized Energy Transfer Rate for YVO_4:Nd^{3+}

TABLE II

TEMPERATURE DEPENDENT INTENSITY RATIOS OF THE TRAP AND HOST SITES FOR 3371Å EXCITATION FOR $YVO_4:Nd^{3+}$

T(K)	t = 0.1 μs I_T/I_H	t = 5.0 μs I_T/I_H
11	0.018	0.340
25	0.051	0.238
40	0.032	0.154
50	0.032	0.143
75	0.035	0.118
100	0.028	0.106
125	0.031	0.108
140	0.037	0.078
160	0.032	0.044
180	0.024	0.098
190	0.021	0.068
200	0.015	0.064

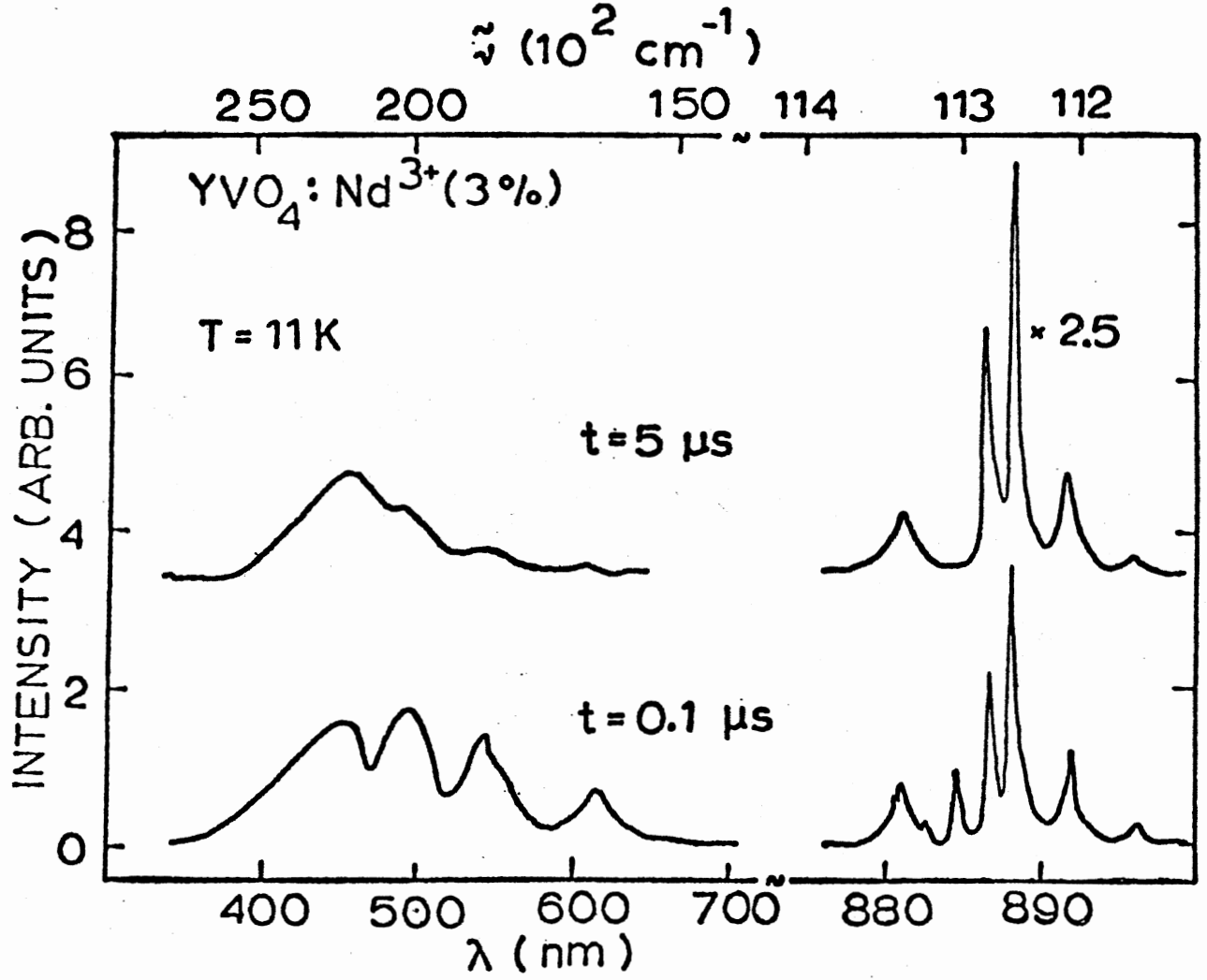

Figure 9. Fluorescence Spectra of YVO_4:Nd^{3+} at Two Times After the Laser Excitation Pulse at 11K

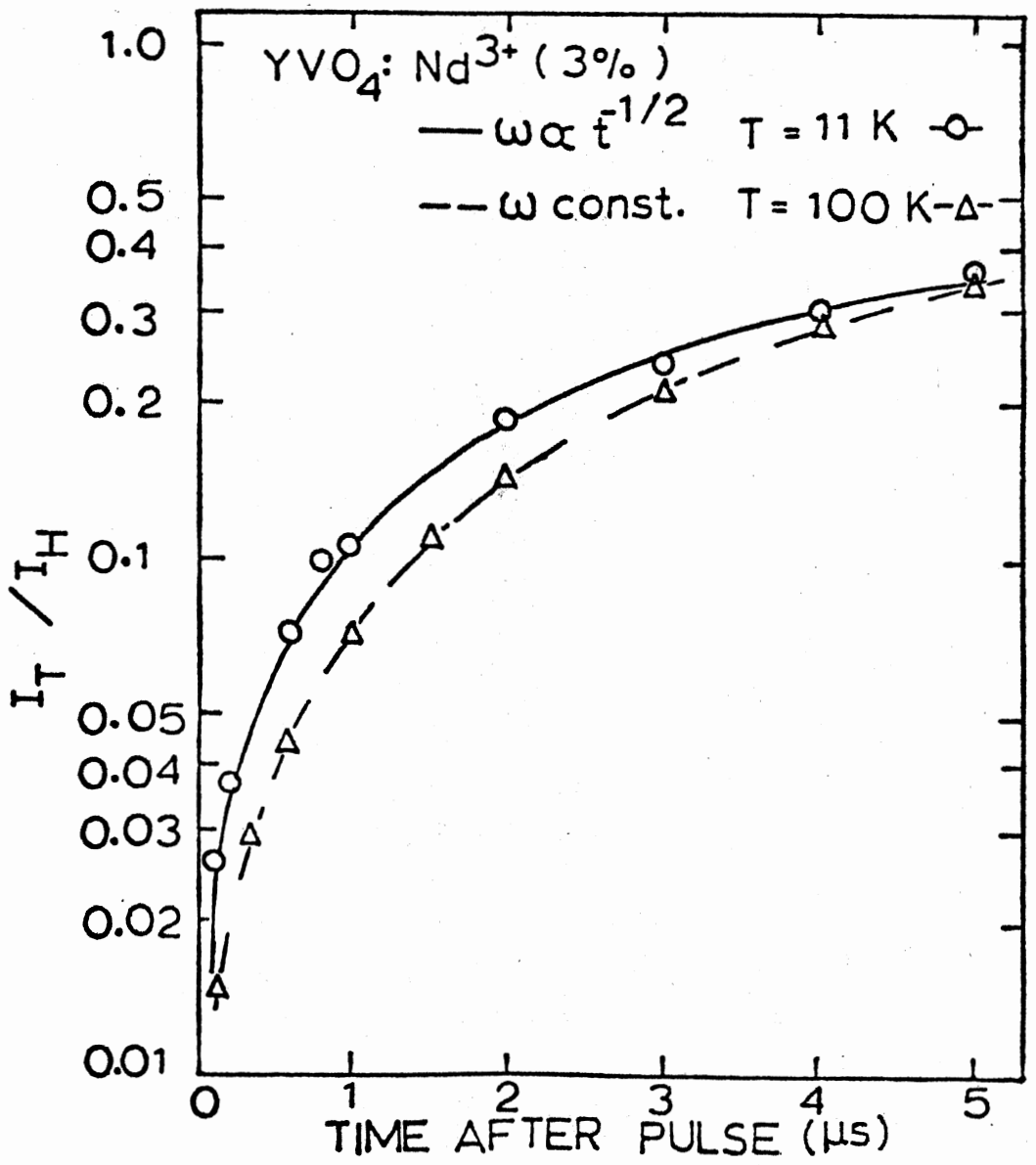

Figure 10. Ratios of the Integrated Fluorescence Intensities of the Nd^{3+} and VO_4^{3-} Emissions as a Function of Time After the Laser Pulse for YVO_4:Nd^{3+}

TABLE III

INTEGRATED FLUORESCENCE INTENSITY RATIOS AT DIFFERENT TIMES AFTER THE LASER PULSE

T = 11 K		T = 100 K	
Time After Pulse (μs)	I_T/I_H	Time After Pulse (μs)	I_T/I_H
0.1	0.018	0.2	0.023
0.4	0.042	0.4	0.033
0.6	0.049	0.6	0.480
0.8	0.092	0.8	0.061
1.0	0.114	1.0	0.084
2.0	0.194	1.5	0.110
3.0	0.235	3.0	0.190
4.0	0.294	4.0	0.241
5.0	0.340	5.0	0.290

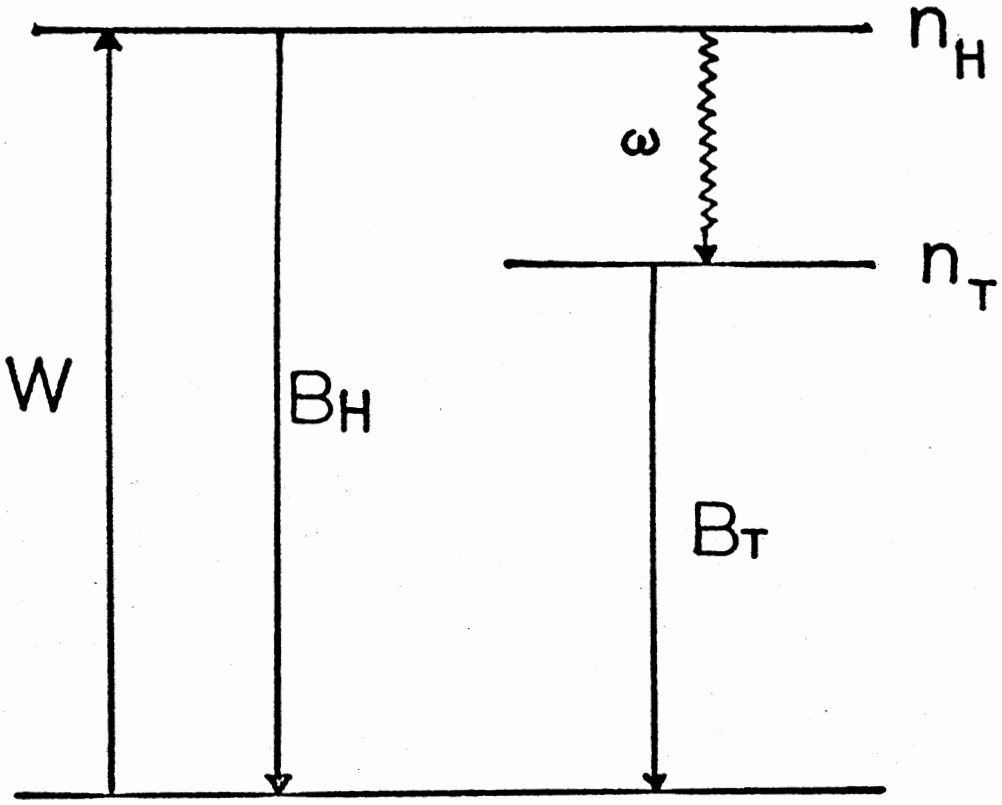

Figure 11. Rate Equation Model for Explaining Host-Sensitized Energy Transfer

These equations can be solved by assuming W to be a delta function in time. Solutions to these equations were obtained fro the two cases: 1) a time-independent energy transfer rate, and 2) a time-dependent energy transfer rate which varied as $t^{-\frac{1}{2}}$. The solutions for n_T and n_H are expressed as a ratio which is proportional to the ratio of the respective integrated fluorescence intensities with a proportionality constant K involving the ratio of the radiative decay rates. Then K and ω were treated as adjustable parameters to obtain the best theoretical fit to the TRS data.

It was found that at low temperatures the theoretical predictions with a time-dependent energy transfer rate gave the best fit to the experimental data. The theoretical fit is shown by the solid line in Figure 10, the parameters being K = 0.10 and $\omega = 8.0 \times 10^2$ $\text{sec}^{-\frac{1}{2}}$. In this case, the solutions to Equations (IV-2) and (IV-3) lead to

$$I_T/I_H = K\left[e^{(B_H-B_T)t + 2\omega t^{\frac{1}{2}}} - \frac{\omega}{(B_H-B_T)t^{\frac{1}{2}} + \omega}\right] \qquad \text{(IV-4)}$$

where

$$\omega = \frac{4}{3}\pi^{3/2} R_o^3 C_T (\tau_H^o t)^{-\frac{1}{2}} \qquad \text{(IV-5)}$$

The expression (IV-5) represents the rate of energy transfer by single-step electric dipole-dipole interaction, where R_o is the critical interaction distance and C_T is the concentration of traps. Using the measured value of the undoped host fluorescence lifetime τ_H^o and the value of ω obtained from theoretical fit to TRS data at 11K gave a value

14.6Å for R_o. A theoretical prediction for R_o can be obtained from the expression

$$R_o = [5.86 \times 10^{-25} \Omega \phi_s^o / (n\tilde{\nu})^4]^{1/6} \qquad \text{(IV-6)}$$

where Ω is the overlap integral of the absorption spectrum of the neodymium ions and the emission spectrum of the host, ϕ_s^o is the quantum efficiency, n is the refractive index, $\tilde{\nu}$ is the average wavenumber in the spectral overlap region, and the numerical factor is for dimensional consistency and contains a factor 2/3 for the average angular dependence of randomly oriented dipoles. The overlap integral Ω is found from measured spectra to be 7.32×10^{-2} liter/mole-cm. A typical illustration to obtain Ω is shown in Figure 12. Using this value for Ω along with $\tilde{\nu} = 2.0 \times 10^{-4}$ cm^{-1}, $\phi_s^o = 0.54$, and n = 1.53, the theoretically predicted value for R_o is found to be 5.5Å.

At high temperatures (about 100K and above) it was found that the best theoretical fit to the experimental data was obtained by assuming a time-independent energy transfer rate. In this case, the theoretical expression for the ratio of integrated fluorescence intensities is found from Equation (IV-2) and Equation (IV-3) to be

$$I_T/I_H = K' \frac{\omega'}{(B_H - \omega' + B_T)} [e^{(B_H + \omega' - B_T)t} - 1] \qquad \text{(IV-7)}$$

The dashed line in Figure 10 represents the best fit to the TRS data at 100K by treating K' and ω' as adjustable parameters with the values of K' = 25 and $\omega' = 2.85 \times 10^3$ sec^{-1}.

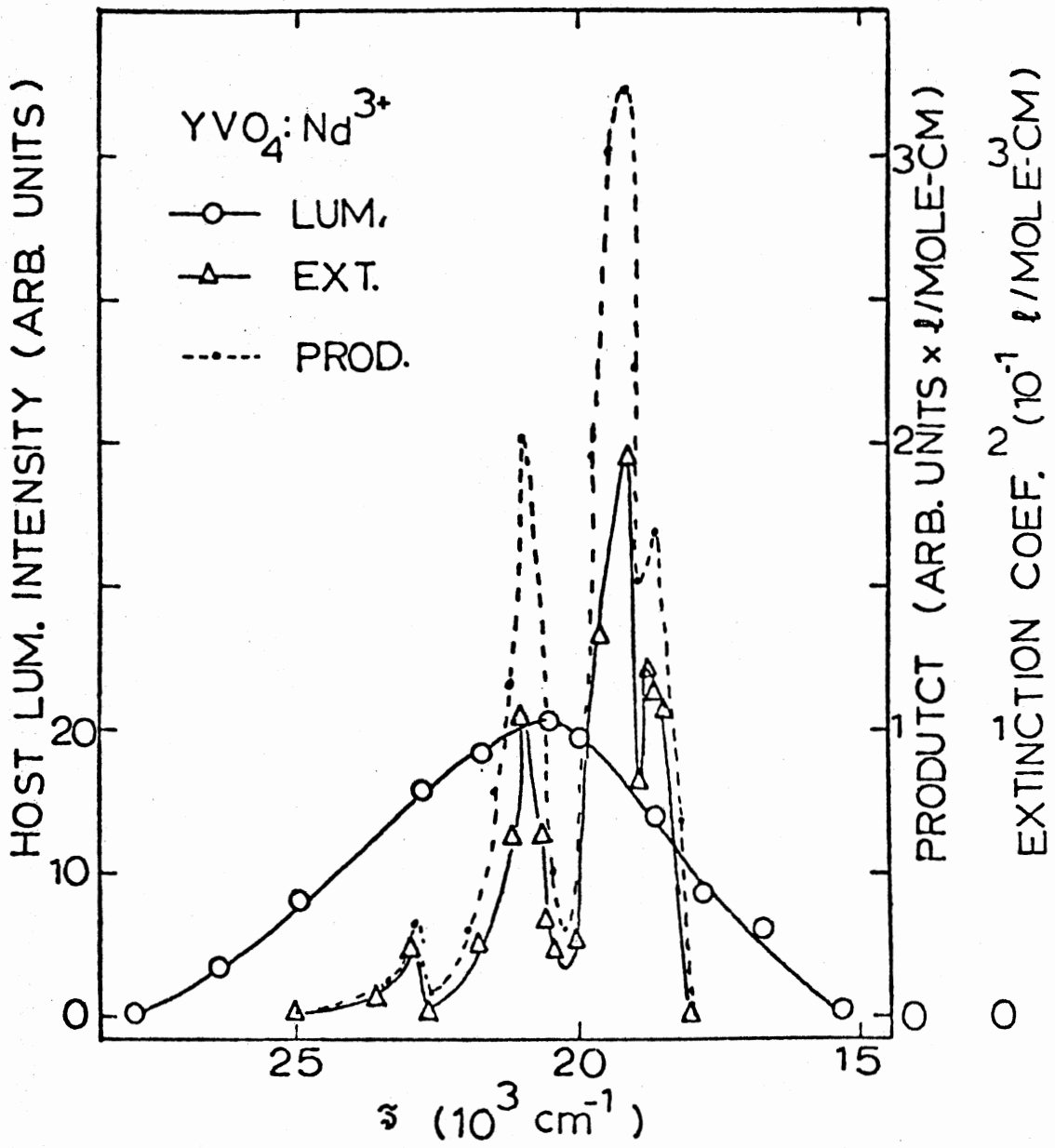

Figure 12. Illustration for the Overlap Integral of Absorption Spectrum of Nd^{3+} and Emission Spectrum of Host Ions

Discussions

The measured values of the fluorescence lifetimes of Nd^{3+} emissions are less than the radiative decay time (24) of 152 μs which indicates that some radiationless quenching is taking place in the system under investigation. At these relatively high concentrations of impurity ions, this kind of quenching is quite probable.

At low temperatures the energy transfer rate was found to be dependent of temperature and vary as $t^{-1/2}$ which indicates that the excitons are self-trapped in this region. On the other hand, the energy transfer rate was found to increase exponentially at high temperatures and be independent of time indicating that thermally activated exciton diffusion is taking place in the crystal at high temperatures. In this temperature region, it appears that emission and absorption of phonons are involved for the conservation of energy.

The multi-step energy migration process at high temperature can be treated by the mathematics of either diffusion or random walk with the resulting energy transfer rate expressed as

$$\omega' = 4 \pi D R_T C_T p \qquad \text{(IV-8)}$$

or,

$$\omega' = V_m C_T C\{A\} t_h^{-1} p \qquad \text{(IV-9)}$$

respectively, where D is the diffusion coefficient, R_T is the trapping radius at the activator site, V_m is the volume per vanadate molecule, t_h is the excitation energy hopping time, $C\{A\}$ is the capacity of the random walk, and p is the probability of the host excitation energy being

transferred to an activator site. Since only one principal experimental parameter ω' is available, the most convenient way to determine the migration and trapping processes is to compare the results obtained from similar experiments (19) on the same host doped with different activators with the assumption that the migration properties of energy transfer should be the same for all samples with only differences in trapping characteristics of different activators. The comparative results obtained for YVO_4 samples containing Eu^{3+}, Er^{3+} and Nd^{3+} are tabulated in Table IV. The similar temperature dependence as shown in Figure 8 was observed (19) in the other samples, but with significant differences in activation energy due to thermal effects being present in both migration and trapping. These differences in activation energies for the host exciton migration in the samples with different traps are due to the absorption and emission of phonons. After adjusting the data to account for the difference in thermal characteristics of the trapping process of activators, the following two ways to interpret the results were attempted.

First, it was assumed that the trapping regions for the three types of activators are all of the same size and the difference in the trapping characteristics is due to p_o. Assuming a point trapping region (28) $C\{A\} = 0.659$ and a trapping radius (R_T) equal to the nearest neighbor Y-V distance of 3.15×10^{-8} cm, the values for p_o were calculated and listed in Table IV. The random walk model predicts an exciton hopping time $t_h = 2.9 \times 10^{-8}$ sec and the diffusion model predicts that $D = 2.6 \times 10^{-8}$ cm^2 sec^{-1}. In the limit of many steps in the random walk the two models should provide the same result which can be verified with the expression

TABLE IV

PARAMETERS OF YVO_4 SAMPLES DOPED WITH THREE DIFFERENT IMPURITY IONS

Parameters	$YVO_4:Nd^{3+}$ (3.8×10^{20} cm^{-3})	$YVO_4:Eu^{3+}$ (1.27×10^{19} cm^{-3})	$YVO_4:Er^{3+}$ (1.27×10^{20} cm^{-3})
R_o (Å)	14	4	2
$\Delta E'$ (cm^{-1})	250	156	1000
ω' (sec^{-1})[a]	4.1×10^{4}	1.0×10^{4}	2.1×10^{5}
$C\{A\}t_h^{-1}p$	2.40×10^{5}	1.75×10^{6}	3.68×10^{6}
$D\ R_T\ p$	8.6×10^{-18}	6.27×10^{-17}	1.32×10^{-16}
p_o	$1. \times 10^{-3}$	7.96×10^{-3}	1

[a] T = 297 K.

$$t_h = \alpha^2/(6D) \qquad \text{(IV-10)}$$

where α is the average hopping distance for excitons. If α is taken to be the shortest V-V separation of 4.75Å and the above mentioned D value is used, the hopping time is found to be 1.5×10^{-8} sec which is consistent with the value obtained from the random walk model. The number of hops in random walk is given by

$$n = \tau_H/t_h \qquad \text{(IV-11)}$$

For $YVO_4:Nd^{3+}$ sample, n was found to be 755.

The second way to interpret the results is to assume that $p_o = 1$ for all three cases; but the sizes of trapping regions for them are quite different from each other. With this assumption R_T for Er^{3+} is of the order of 1,830Å which is unphysically large. It also predicts such a slow hopping time that only one hop could take place in a random walk which is not consistent with the observed time-independent energy transfer rate. Therefore, the first approach was concluded to be correct interpretation of the results.

The diffusion length at room temperature was determined by the expression

$$\ell = \sqrt{2D\tau_H^o} \qquad \text{(IV-12)}$$

and was found to be 8.8×10^{-7} cm. The diffusion coefficient can be expressed as

$$D = D_o e^{-\Delta E_h/kT} \qquad \text{(IV-13)}$$

where ΔE_h is the activation energy for hopping. The value of D_o was found to be 5.4×10^{-7} cm^2 sec^{-1}. The exciton migration and trapping parameters for the $YVO_4:Nd^{3+}$ system is listed in Table V.

In this model, the host excited states involve charge transfer transitions and are localized on a vanadate molecular ion. This can be treated as a Frenkel exciton which is self-trapped at low temperatures and undergoes thermally activated hopping among the other VO_4^{3-} ions at high temperatures. Table IV shows that there are significant differences in the thermal activation energies and the trapping probabilities per visit to an activator site in the YVO_4 samples doped with Eu^{3+}, Er^{3+} and Nd^{3+} ions. The reason for the difference is still unknown, but it is important to note that they increase with increasing number of 4f electrons and decreasing ionic radius.

The measured value of R_o for Nd-doped samples was found to be significantly larger than for other activators in the same host material and also much larger than the theoretically predicted value . The reason for this discrepancy is not understood at this moment. More work along this line needs to be done to have better understanding.

TABLE V

EXCITON MIGRATION AND TRAPPING PARAMETERS ALONG WITH MODEL FITTING PARAMETERS

Parameter	$YVO_4:Nd^{3+}$ (3.8×10^{20} cm^{-3})
$D(cm^2\ sec^{-1})$ [a]	2.6×10^{-8}
ℓ (cm)	8.8×10^{-7}
t_h (sec)	2.9×10^{-2}
n (hop)	755
R_T (cm)	3.15×10^{-8}
K	0.10
K'	25
ω ($sec^{-\frac{1}{2}}$)	8.0×10^{2}
ω' (sec^{-1})	2.85×10^{3}

[a] T = 297 K.

CHAPTER V

SITE-SELECTION SPECTROSCOPY OF Nd^{3+} IONS IN $YVO_4:Nd^{3+}$ AND $Nd\,Al_3(BO_3)_4$ CRYSTALS

A thorough investigation has been made on energy transfer among trivalent neodymium ions in yttrium vandate host and neodymium aluminum borate (NAB) crystals. The high resolution tunable dye laser described in Chapter III was employed to directly excite the Nd^{3+} ions present in specific crystal field sites. The high concentrations of active ions in these crystals allow ion-ion interaction resulting in energy migration among these ions which can again be characterized by time-resolved spectroscopy techniques.

Results and Interpretation of $YVO_4:Nd^{3+}$ Data

When Nd^{3+} ions were selectively excited with a dye laser using rhodamine 6G dye, a definite structure of each of the sharp lines of the Nd^{3+} emissions was observed. This structure is attributed to emission from ions in nonequivalent types of crystal field sites and it changes with laser excitation wavelength due to the selective excitation of ions in different sites as shown in Figure 13.

In order to study energy transfer among trivalent neodymium ions, the fluorescence spectra of their sharp emission lines were recorded at different times after the laser pulse. A typical emission spectrum near 888 nm for two different times after laser excitation of 5874Å and

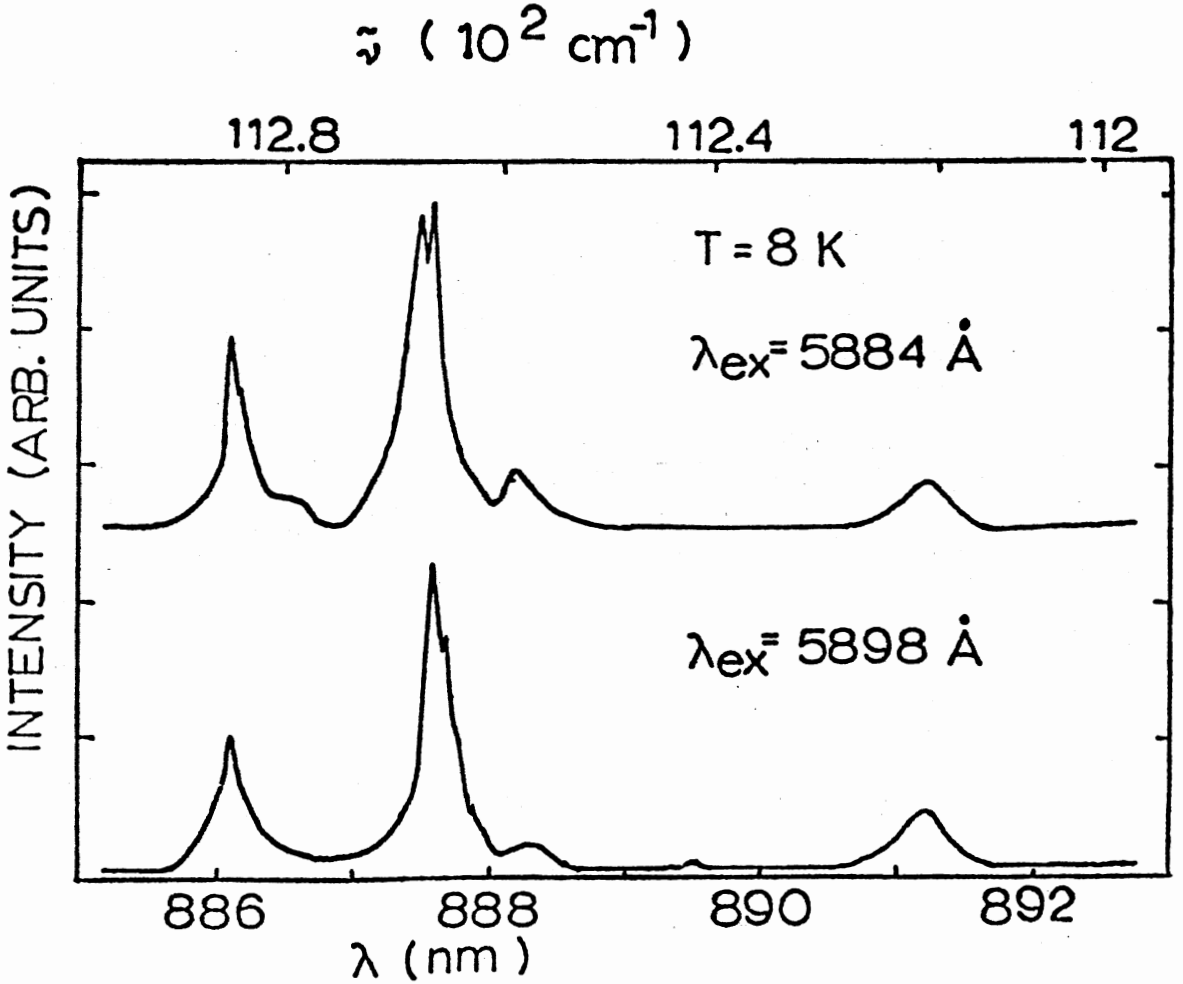

Figure 13. Fluorescence Spectra of Nd^{3+} in YVO_4:Nd^{3+} for Two Different Wavelengths of Laser Excitation at 11K

observed at 8K is shown in Figure 14, where it is seen that the high energy structure decreases while the low energy structure increases with time after the laser pulse due to energy transfer. Designating the ions responsible for the high energy structure for appropriate transitions as "sensitizers" and those for low energy structure as "activators", energy transfer between them can be characterized by plotting the ratio of the integrated fluorescence intensities as a function of time after the laser pulse. These TRS results observed at 8K and 100K are shown in Figure 15 and tabulated in Table VI.

A quantitative interpretation of the TRS data can be given using the proposed theoretical model shown in Figure 16, which is similar to the model used in Chapter IV to analyze the host-sensitized energy transfer results with the exception that direct excitation of activators is allowed and no significant difference was detected in the fluorescence lifetimes of sensitizers and activators. The excited state populations are designated as n_s and n_a for sensitizers and activators respectively. W_s and W_a are the direct pumping rates for these levels while B represents their decay rates. The energy transfer rate between them is designated by ω_{sa}. The rate equations for the excited state populations are given by

$$dn_s/dt = W_s - Bn_s - \omega_{sa} n_s \qquad (V\text{-}1)$$

$$dn_a/dt = W_a + \omega_{sa} n_s - Bn_a \qquad (V\text{-}2)$$

These equations can be solved assuming delta function excitation and a specific time-dependence for the energy transfer rate. The best theoretical fits to the data at all temperatures were obtained with time-

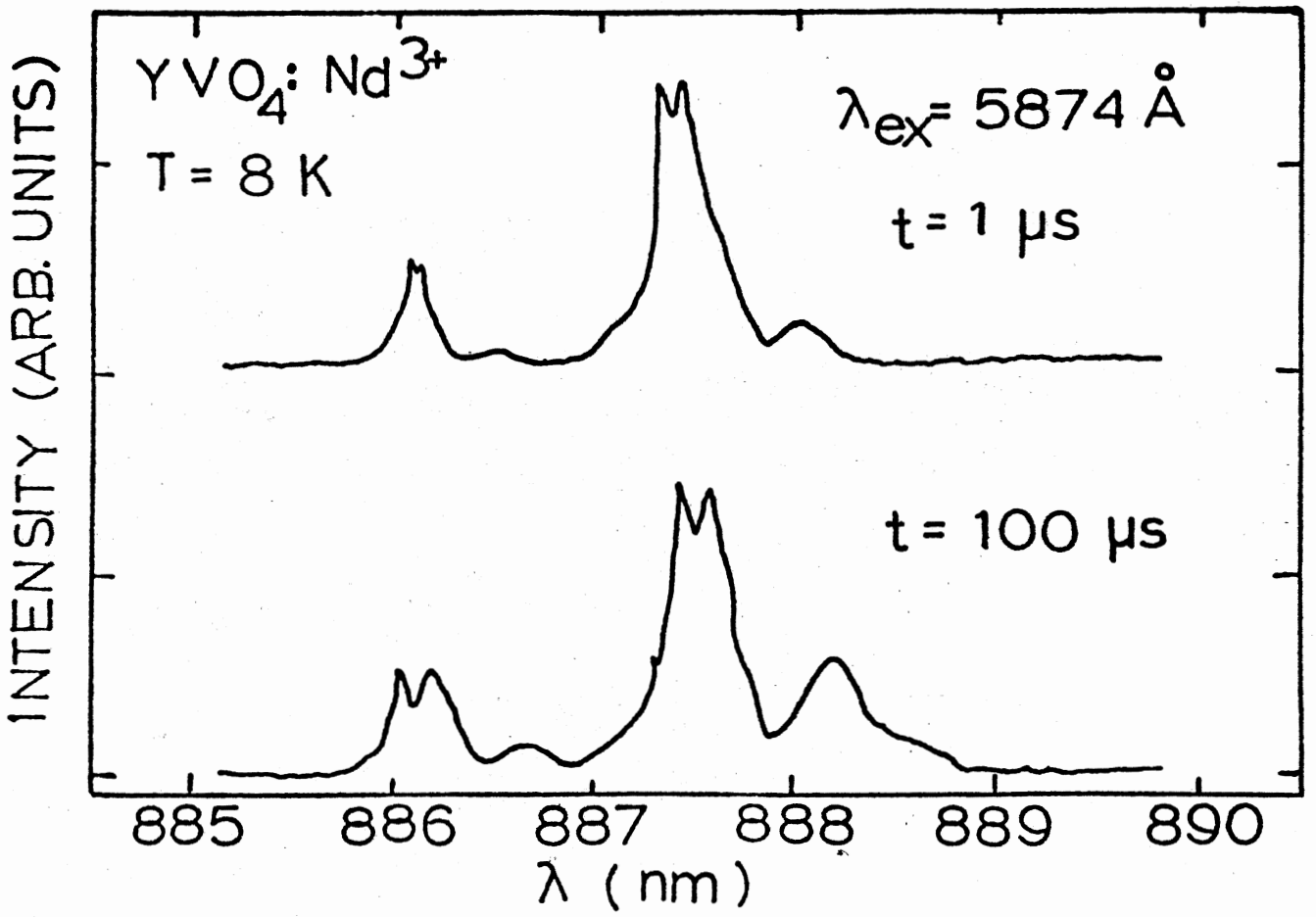

Figure 14. Fluorescence Spectra of Nd^{3+} in YVO_4:Nd^{3+} at Two Times After the Laser Pulse

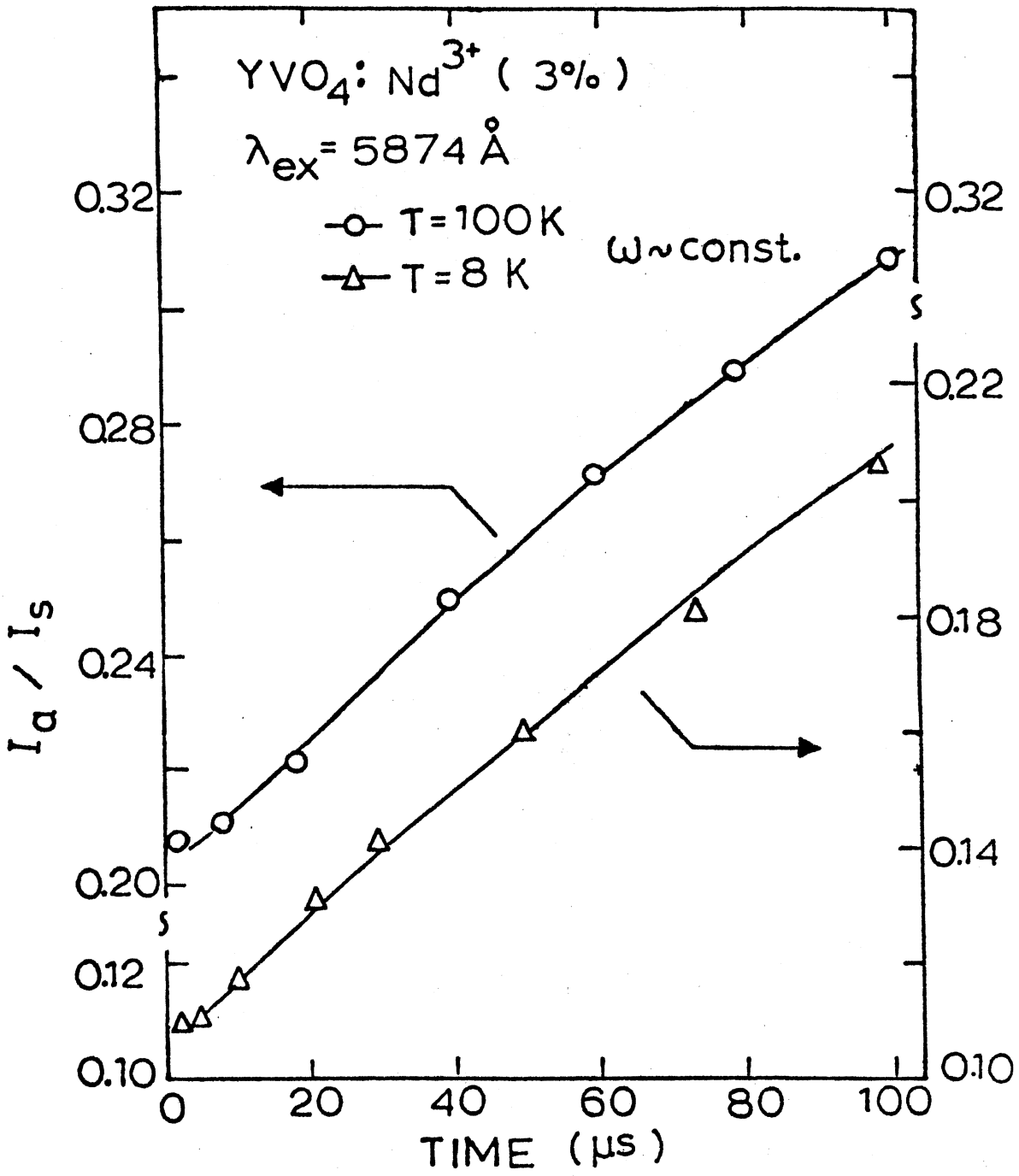

Figure 15. Ratios of the Integrated Fluorescence Intensities of Sensitizer and Activator Nd^{3+} Ions as a Function of Time After the Laser Pulse for $YVO_4:Nd^{3+}$. (See Text for Explanation of Theoretical Line)

TABLE VI

INTEGRATED FLUORESCENCE INTENSITY RATIOS FOR 8882Å AND 8875Å LINES OF $YVO_4:Nd^{3+}$ AT DIFFERENT TIMES AFTER THE LASER PULSE

T = 8K		T = 100K	
Time After Laser Pulse (μs)	$\frac{I_{8882}}{I_{8875}}$	Time After Laser Pulse (μs)	$\frac{I_{8882}}{I_{8875}}$
1	0.109	5	0.210
5	0.112	10	0.220
10	0.117	15	0.235
15	0.130	20	0.260
30	0.150	30	0.280
50	0.170	40	0.290
75	0.180	50	0.300
100	0.200		

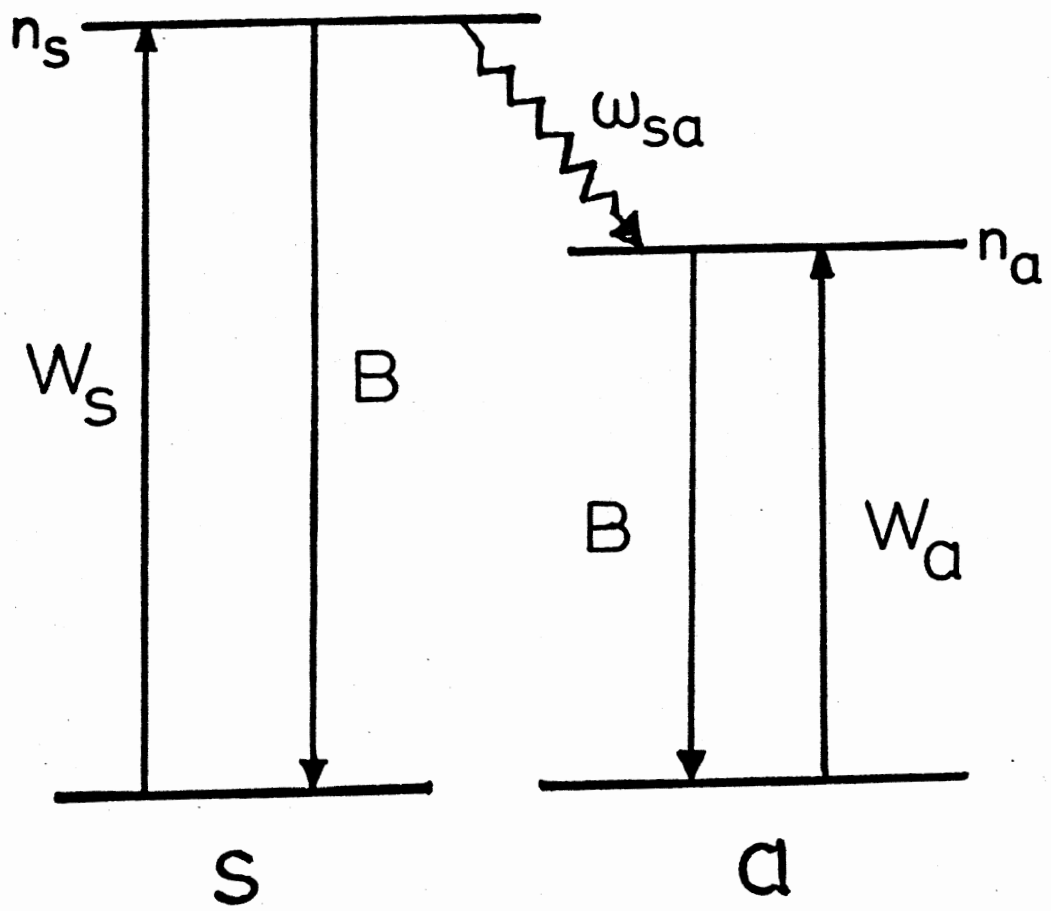

Figure 16. Rate Equation Model for Explaining Energy Transfer Between Nd^{3+} Ions in YVO_4:Nd^{3+}

independent energy transfer rates. For this case, the solutions to Equations (V-1) and (V-2) lead to

$$I_a/I_s = K'' \left[\{ n_a^{(o)}/n_s^{(o)} + 1 \} e^{\omega_{sa} t} - 1 \right] \qquad \text{(V-3)}$$

where $n_s^{(o)}$ and $n_a^{(o)}$ are the initial excited populations from the pumping. K" is the proportionality constant involving the ratio of radiative emission rates. K", $n_a^{(o)}/n_s^{(o)}$, and ω_{sa} were treated as adjustable parameters to obtain the best fits as shown by solid lines in Figure 15, with the values of k" = 0.098, $n_a^{(o)}/n_s^{(o)} = 1.1$, and $\omega_{sa} = 4 \times 10^{-3}$ μs^{-1} for 8K; and k' = 0.098, $n_a^{(o)}/n_s^{(o)} = 2.1$ and $\omega_{sa} = 6 \times 10^{-3}$ μs^{-1} for 100K.

The temperature dependence of the energy transfer rate can be obtained using Equation (V-3) and the integrated fluorescence ratios at short and long times after the excitation pulse. The integrated fluorescence intensity ratios at short and long times after the laser excitation at 5874Å observed at different temperatures are listed in Table VII. Using this table and Equation (V-3) the energy transfer rates were obtained and listed in Table VIII and shown in Figure 17. The transfer rate remains approximately constant at low temperatures and increases significantly at high temperatures (about 25K or above). The activation energy for this increase is found to be about 15 cm^{-1} which is essentially the same as the crystal field splitting of the metastable $^4F_{3/2}$ level in this system.

The temperature dependence is the key for understanding the energy transfer between neodymium ions and is consistent with a two-phonon-assisted energy transfer process suggested by Holstein, Lyo and Orbach (29). The energy transfer rate between ions i and j for the resonance-

TABLE VII

TEMPERATURE DEPENDENT INTEGRATED FLUORESCENCE INTENSITY RATIOS AT SHORT AND LONG TIMES AFTER THE LASER PULSE OF 5874Å FOR $YVO_4:Nd^{3+}$

T(K)	$\frac{t = 1\ \mu s}{I_{8881}/I_{8875}}$	$\frac{t = 100\ \mu s}{I_{8881}/I_{8875}}$
8	0.10	0.20
15	0.105	0.20
25	0.12	0.22
30	0.11	0.23
35	0.11	0.26
40	0.13	0.28
50	0.13	0.33
60	0.16	0.37
70	0.16	0.41
75	0.21	0.44

TABLE VIII

TEMPERATURE DEPENDENT ENERGY TRANSFER RATES FOR $YVO_4:Nd^{3+}$

T(K)	ω_{sa} (μs^{-1}) (k''' = 0.098)
8	3.9×10^{-3}
15	3.88×10^{-3}
25	3.81×10^{-3}
30	4.3×10^{-3}
35	5.48×10^{-3}
40	5.56×10^{-3}
50	5.90×10^{-3}
60	6.02×10^{-3}
70	6.84×10^{-3}

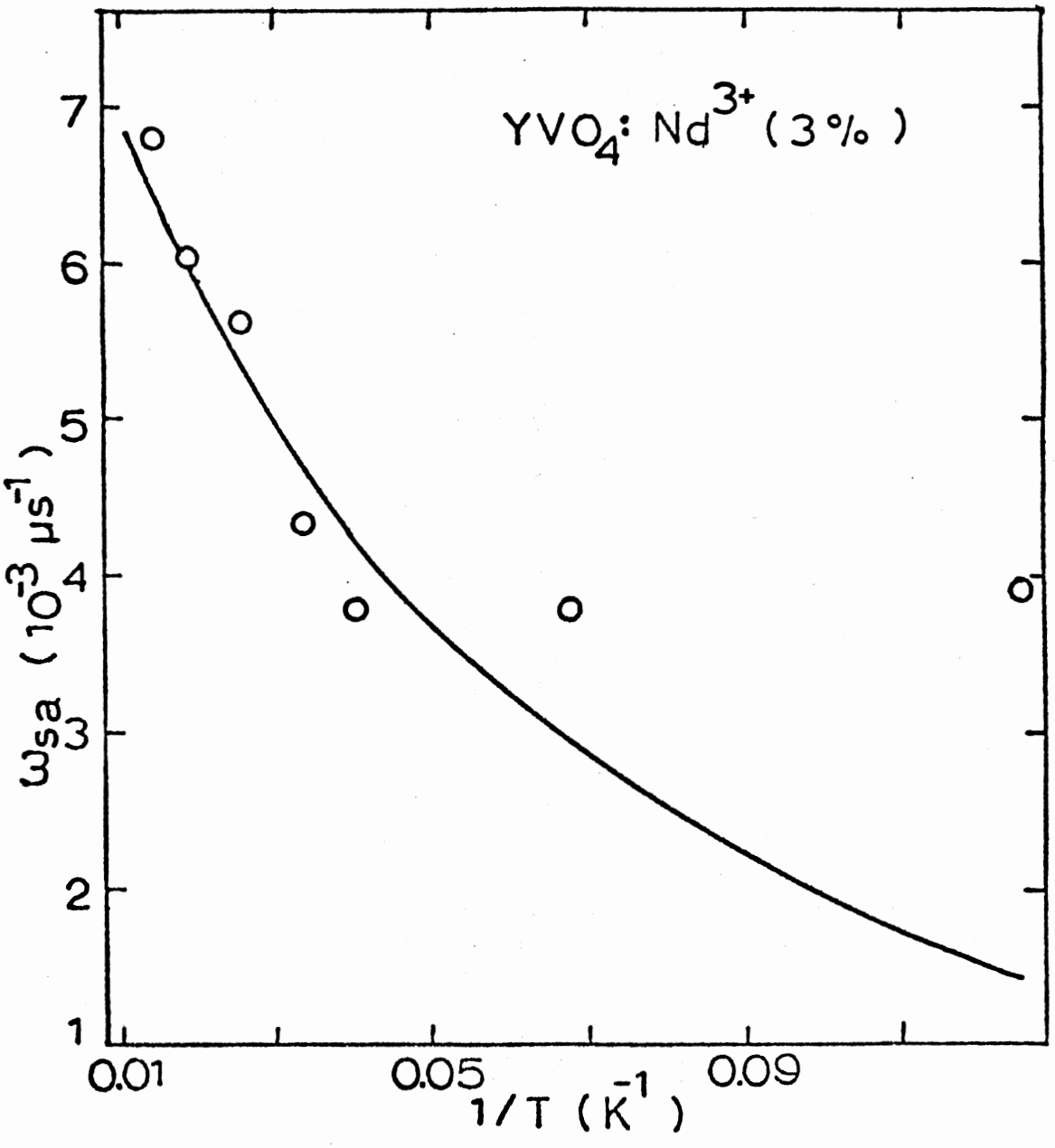

Figure 17. Temperature Dependence of the Rate of Energy Transfer Between Nd^{3+} Ions in YVO_4:Nd^{3+}. (See Text for Explanation of Theoretical Line)

phonon-assisted transfer process is given by (29)

$$W_{res} = \left[J_1^2 + J_2^2 \frac{2(\Delta E_{ij})^2}{(\Delta E_{ij})^2 + 8\Gamma^2}\right] \times \left[1 + e^{\Delta E_{ij}/kT}\right] \times \left[\frac{2\Gamma}{\pi(\Delta E_{ij})^2}\right] e^{-\delta/kT} \qquad (V\text{-}4)$$

where J_1 and J_2 are the matrix elements representing ion-ion interaction strengths for transfer involving the initial excited state and the ground state and for transfer involving the intermediate state reached by the phonons respectively, ΔE_{ij} represents the energy mismatches between the transitions of respective pair of ions involved in transfer process, Γ is the width of the intermediate state reached by phonons and δ is the energy of the resonant phonons. As already mentioned in Chapter II, at long times after the excitation pulse the diffusion-limited energy transfer case is obtained and the rate is given by (5)

$$\omega_s = 4 \pi D C_a R_T \qquad (V\text{-}5)$$

where

$$R_T = 0.676 W_{sa}^{1/4} R_{sa}^{3/2} D^{-1/4} \qquad (V\text{-}5a)$$

is the trapping radius and D is diffusion coefficient the expression of which was given by Trlifaj (7) as

$$D = 3.4 C_s^{4/3} R_{ss}^6 W_{ss} \qquad (V\text{-}5b)$$

where W's are the energy-transfer interaction strengths and R's are the nearest-neighbor distances between respective pair of ions. Assuming ΔE_{ss} to be small compared with Γ and kT, and using Equations (V-4) and

and (V-5), the final expression for the rate of energy transfer is obtained as

$$\omega_{sa} = 71.6\, C_a\, C_s\, R_{Nd}^{6} \left(\frac{\Gamma}{\hbar}\right) \left[1 + e^{\Delta E_{sa}/kT}\right]^{1/4}$$

$$\times \left[\frac{J_1^2}{\Delta E_{ss}} + \frac{J_2^2}{4\Gamma^2}\right]^{3/4}$$

$$\times \left[\frac{J_1^2}{\Delta E_{sa}^2} + \frac{2J_2^2}{\Delta E_{sa}^2 + 8\Gamma^2}\right]^{1/4} e^{-\delta/kT} \qquad \text{(V-6)}$$

In the case of $YVO_4:Nd^{3+}$ samples ΔE_{sa} is measured to be about 7.9 cm^{-1} and ΔE_{ss} is taken to be about one-third of the inhomogeneous linewidth of the sensitizer transition which is about 1.6 cm^{-1}. δ is the energy of the resonant phonons required to change the ion from the initial to the intermediate state. In this case, the intermediate state happens to be the upper crystal field component of $^4F_{3/2}$ level and so δ is 15 cm^{-1}. Γ is the width of the intermediate state reached by phonons and is measured to be 4.9 cm^{-1}. The squared matrix elements can be expressed in terms of Judd-Ofelt parameters Ω as (31)

$$J^2 = \frac{(2/3)\,(e^2/R_{Nd}^3)^2}{(2J_s+1)(2J_a+1)} \times \left[\sum_k \Omega_{sk} \left|\langle J_s \| U^{(k)} \| J_s' \rangle\right|^2\right]$$

$$\times \left[\sum_k \Omega_{ak} \left|\langle J_a \| U^{(k)} \| J_a' \rangle\right|^2\right] \qquad \text{(V-7)}$$

where R_{Nd} is the average separation between two Nd^{3+} ions and found to be 8.56×10^{-8} cm in this system. The summations over the reduced matrix elements were evaluated for $^4F_{3/2}$ to $^4I_{9/2}$ transitions of Nd^{3+}

ions in yttrium vanadate host and were found (24) to be

$$J_1^2 = 4.15 \times 10^{-50} R_{Nd}^{-6} \text{ cm}^4$$
$$J_2^2 = 9.41 \times 10^{-50} R_{Nd}^{-6} \text{ cm}^4 \quad \text{(V-8)}$$

where the population differences between two components of the $^4F_{3/2}$ level were taken into account. For the particular sites investigated in $YVO_4:Nd^{3+}$, the concentrations found from their relative intensities were $C_s = 3.6 \times 10^{20}$ cm^{-3} and $C_a = 1.8 \times 10^{19}$ cm^{-3}. With all these considerations, Equation (V-6) predicts theoretical values for the energy transfer rate at different temperatures shown as a solid line in Figure 17. The theoretical predictions give a good bit to the data at high temperatures, but the predicted values are smaller than those observed at low temperatures. The parameters for this theoretical model are listed in Table IX.

Discussions on $YVO_4:Nd^{3+}$ Results

It was found that the results obtained in this system were consistent with a multistep diffusion type of energy transfer with the mechanisms for diffusion and trapping both involving two-phonon-assisted processes. The value of the diffusion coefficient for energy migration among the Nd^{3+} ions in YVO_4 host is given by (22).

$$D = 3.4\, C_s^{4/3} R_{ss}^6 \left[J_1^2 + J_2^2 \frac{2(\Delta E_{ss})^2}{(\Delta E_{ss})^2 + 8\Gamma^2}\right] \times \left[\frac{2\Gamma}{\hbar(\Delta E_{ss})^2}\right] \times \left[1 + e^{\Delta E_{ss}/kT}\right] e^{-\delta/kT} \quad \text{(V-9)}$$

TABLE IX

PARAMETERS FOR ION-ION INTERACTION ENERGY TRANSFER MECHANISM AMONG Nd^{3+} IONS IN μVO_4

Parameters	$YVO_4:Nd^{3+}$ (3.8×10^{20} cm^{-3})
C_s (cm^{-3})	3.6×10^{20}
C_a (cm^{-3})	1.8×10^{19}
ΔE_{ss} (cm^{-1})	1.6
ΔE_{sa} (cm^{-1})	7.9
δ (cm^{-1})	15
Γ (cm^{-1})	4.9
$J_1^2 R_{Nd}^6$ (cm^4)	4.15×10^{-50}
$J_2^2 R_{Nd}^6$ (cm^4)	9.41×10^{-50}
R_{Nd} (cm)	8.56×10^{-8}
D (cm^2 sec^{-1})[a]	1.3×10^{-12}
ω_{sa} (μs^{-1})[b]	6.3×10^{-3}

[a] $T = 295$ K.

[b] $T = 75$ K.

and found to be 1.3 x 10^{-12} cm^2 sec^{-1} at 295K. This value is somewhat smaller in this host than in the garnet hosts (30,32) due to the increased value of inhomogeneous broadening of the transitions.

A previous site-selection spectroscopy investigation performed on YVO_4:Eu^{3+} (1%) crystals (19) showed that the results were consistent with energy transfer by a single-step resonant electric dipole-dipole interaction process. One of the reasons for the significant difference in energy transfer processes for different impurity ions could be due to the much higher concentration of Nd^{3+} ions in YVO_4:Nd^{3+} (3%) crystals.

The poor agreement between theory and observation at low temperatures indicates that other energy transfer processes are, perhaps, becoming prominant at these temperatures. It should, however, be pointed out that the agreement is quite good at high temperatures, becasue there are no adjustable parameters in the theoretical prediction.

A Monte Carlo computer simulation technique (14) was also used to fit the data with the assumption that the excitons are hopping on a lattice of randomly distributed sites. A good fit to the TRS data at 100K is shown in Figure 18, where the solid line represents the TRS results and the circles represent the predictions of the Monte-Carlo approach with the critical interaction distance of R_o = 26Å. This is excidingly large compared to the value obtained by theoretical prediction. The discrepancy may arise due to the longer hopping times in the Monte-Carlo approach dominating over the shorter ones.

Results and Interpretation of Nd $Al_3(BO_3)_4$ Data

Investigation of the mechanisms of energy transfer among Nd^{3+} ions in neodymium aluminium borate crystals was done by using the same

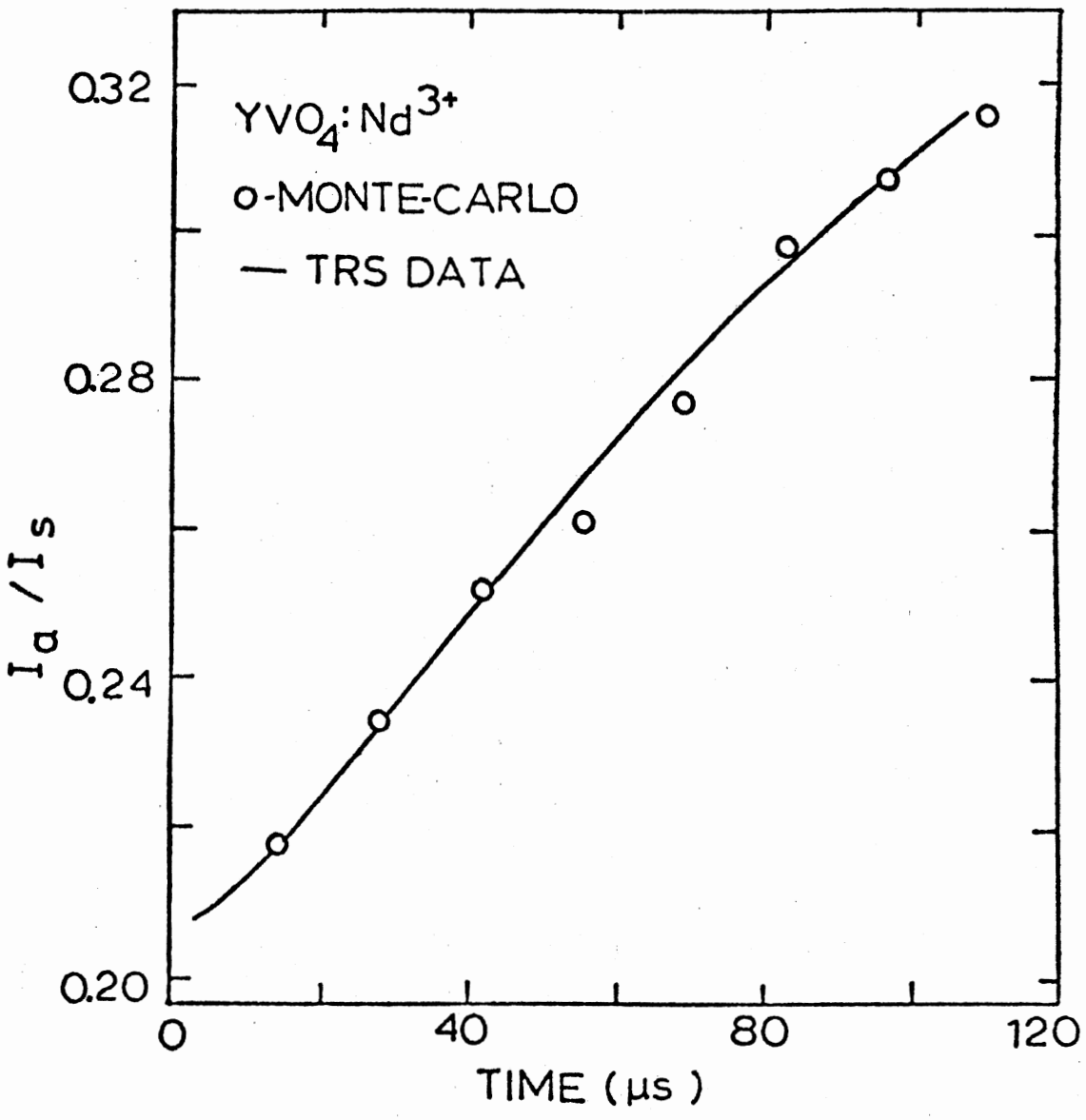

Figure 18. Fitting of the Estimates of a Monte-Carlo Computer Simulation Technique With TRS Data for $YVO_4:Nd^{3+}$ at 100K

technique as used for the studies of $YVO_4:Nd^{3+}$ samples. The fluorescence spectra of Nd $Al_3(BO_3)_4$ at 11K in the region from about 8800 to 8900Å are shown in Figure 19, for two excitation wavelengths of 5919 and 5925Å. The definite structure of the lines from each transition varies significantly with the excitation wavelength due to the presence of ions in nonequivalent crystal field sites. The lifetime of Nd^{3+} fluorescence in this sample was found to be about 20 μs and independent of temperature.

Energy transfer in this sample was investigated with time-resolved site-selection spectroscopy methods as before. Figure 20 shows a pair of typical spectra for two times after the laser pulse for the excitation wavelength of 5919Å observed at 11K. The high energy structure decreases while the low energy structure increases with time after the laser pulse due to energy transfer from ions in the sites producing the low energy transitions to ions in the sites producing the high energy transitions. The qualitative analysis for energy transfer is obtained by plotting the integrated fluorescence intensity ratios of activator and sensitizer transitions versus time after the laser pulse shown in Figure 21 and the results are tabulated in Table X for 11K and 40K. At higher temperatures the fluorescence lines were broadened to such an extent that the transitions from ions in slightly different crystal field sites could not be resolved precisely.

The TRS data was interpreted using the same phenomenological rate parameter model shown in Figure 16, as before. In this case the best fit to the data was obtained with time-dependent energy transfer rate which varied as $t^{-\frac{1}{2}}$ as both low and high temperatures. The solutions to the rate Equations (V-1) and (V-2), in this case, give

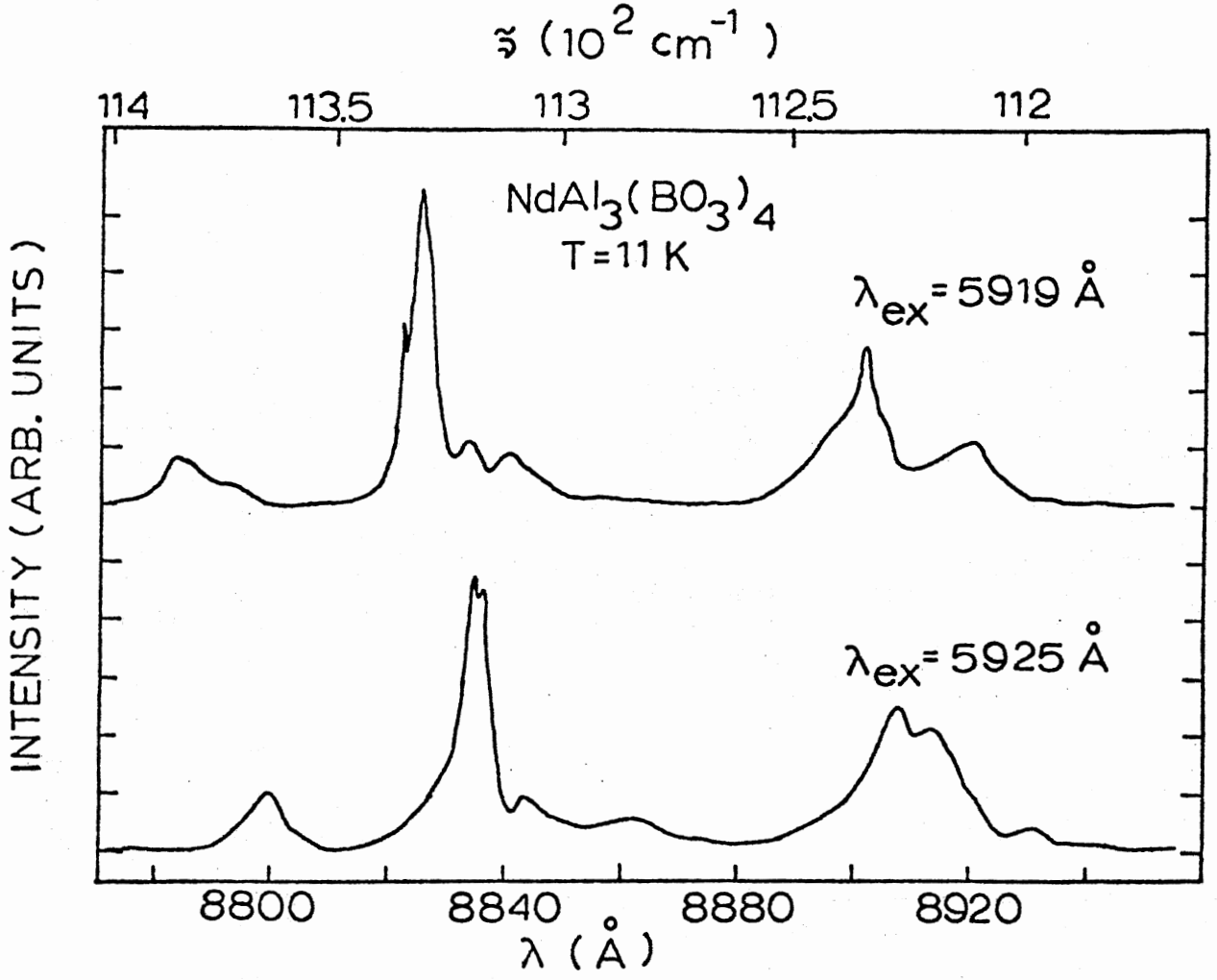

Figure 19. Fluorescence Spectra of $NdAl_3(BO_3)_4$ at Two Different Excitation Wavelengths at 11K

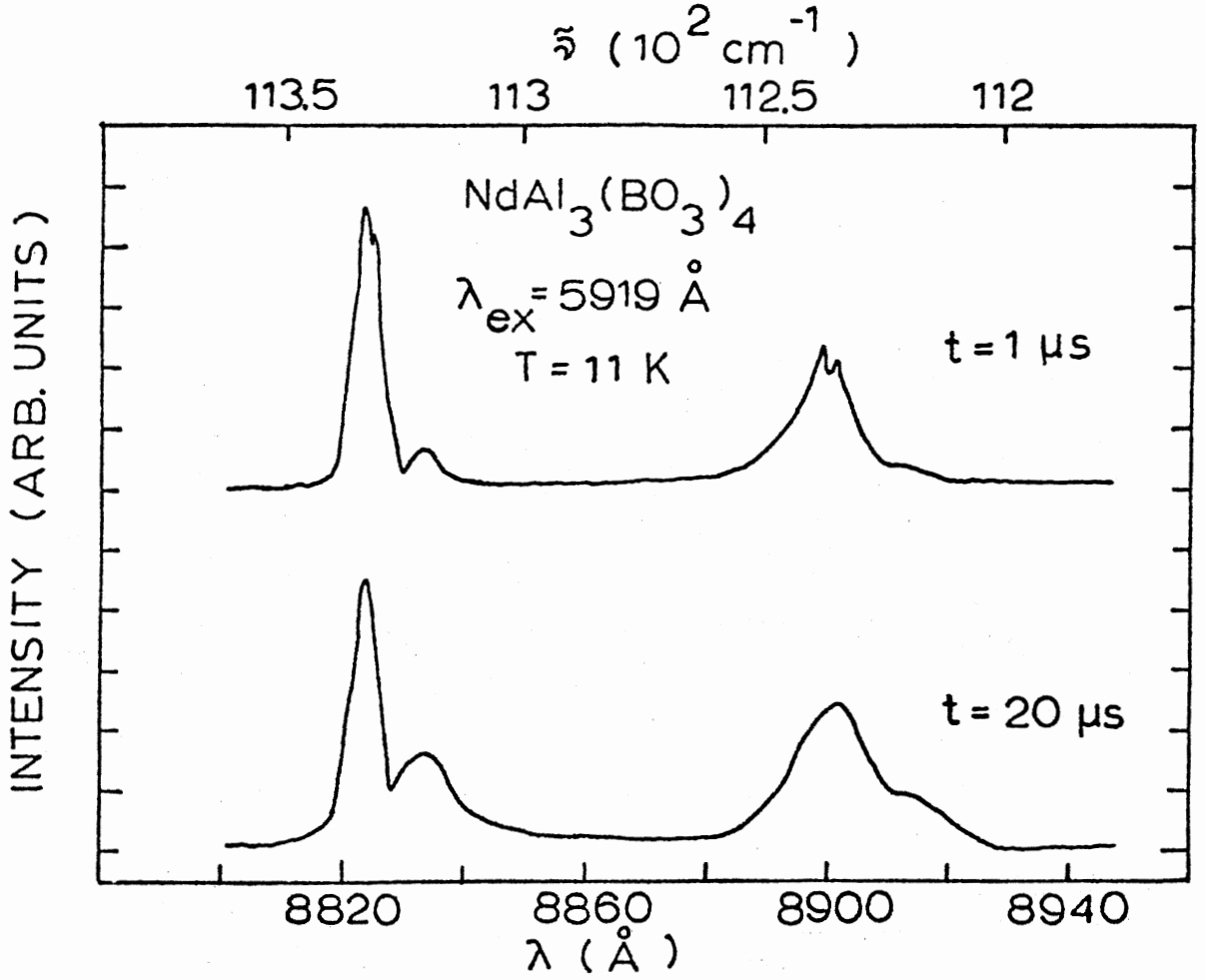

Figure 20. Fluorescence Spectra of $NdAl_3(BO_3)_4$ at Two Times After the Laser Pulse at 11K

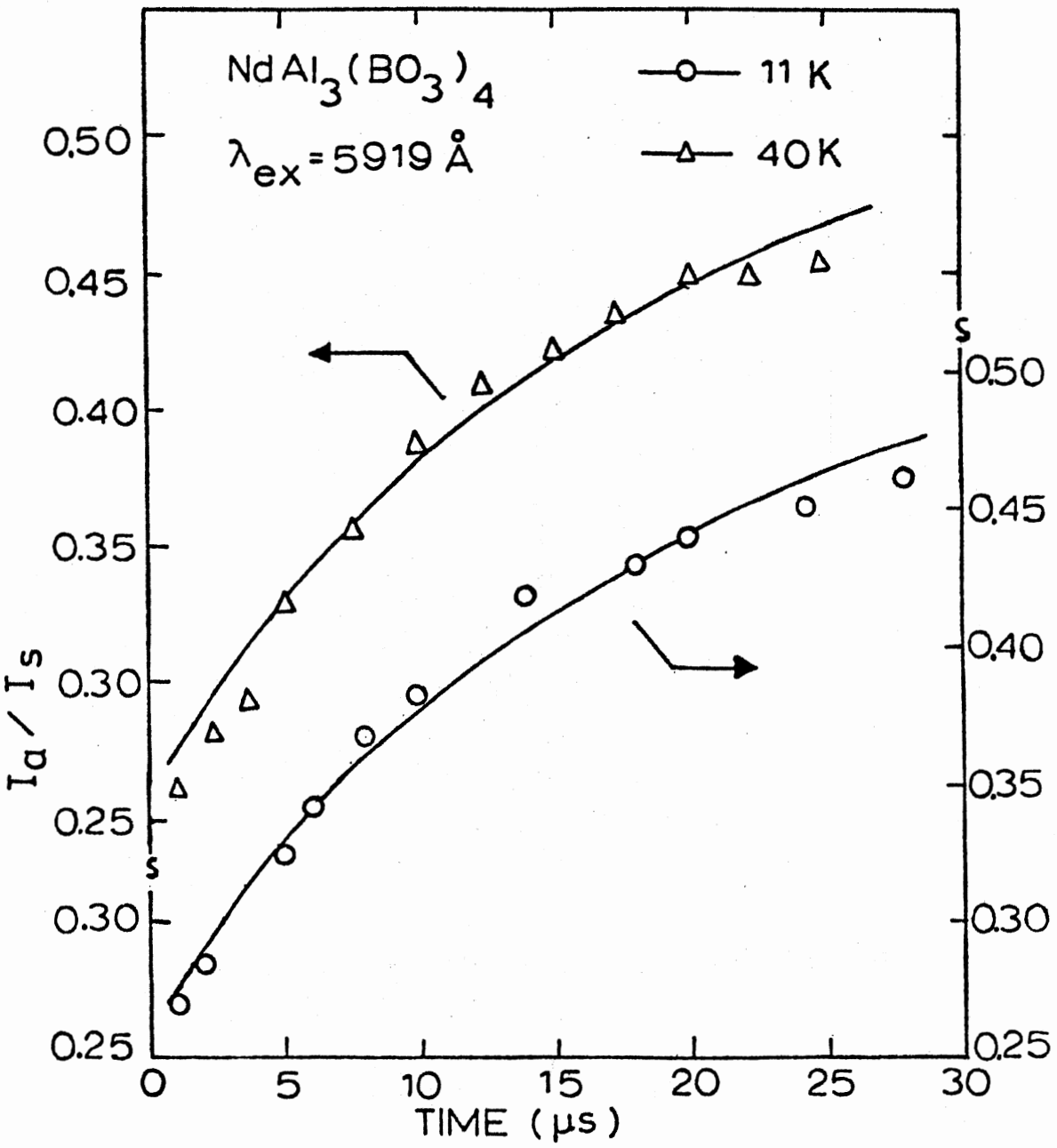

Figure 21. Ratios of the Integrated Fluorescence Intensities of Activator and Sensitizer Transitions as a Function of Time After the Laser Excitation Pulse for $NdAl_3(BO_3)_4$. (See Text for Explanation of Theoretical Line)

TABLE X

INTEGRATED FLUORESCENCE INTENSITY RATIOS FOR 8834Å AND 8825Å LINES OF Nd $Al_3(BO_3)_4$ AT DIFFERENT TIMES AFTER THE LASER PULSE

T = 11K		T = 40K	
t(μs)	I_{8834}/I_{8825}	t(μs)	I_{8834}/I_{8825}
1.0	0.270	0.5	0.260
2.0	0.285	1.0	0.260
4.0	0.334	2.0	0.280
5.0	0.323	3.0	0.285
6.0	0.340	4.0	0.333
8.0	0.368	5.0	
10.0	0.385	6.0	0.359
12.0	0.390	8.0	0.390
14.0	0.420	10.0	0.410
16.0	0.420	12.0	0.420
18.0	0.430	14.0	0.434
20.0	0.440	16.0	0.450
24.0	0.450	18.0	0.450
28.0	0.460	20.0	0.453

$$I_a/I_s = k''' \left[\{n_a^{(o)}/n_s^{(o)} + 1\} e^{\omega t^{\frac{1}{2}}} - 1\right] \qquad \text{(V-10)}$$

where $\omega = 2\omega_{sa} t^{\frac{1}{2}}$ and k''' is proportionality constant involving radiative decay rates. The solid lines in Figure 21 represent the best theoretical fits to the data treating k''', $n_a^{(o)}/n_s^{(o)}$, and ω as adjustable parameters with the values of $k''' = 0.16$, $n_a^{(o)}/n_s^{(o)} = 1.2$, and $\omega = 4.0 \times 10^{-2}\ \mu s^{-\frac{1}{2}}$ for T = 11K; and $k''' = 0.21$, $n_a^{(o)}/n_s^{(o)} = 1.1$, and $\omega = 9.5 \times 10^{-2}\ \mu s^{-\frac{1}{2}}$ for T = 40K.

The temperature dependence of energy transfer rate was determined by measuring the fluorescence intensity ratios for certain time after the laser pulse at different temperatures. The results are shown in Figure 22 and listed in Table XI. The transfer rate appeared to be independent of temperature at temperatures below about 25K and began to increase exponential at higher temperatures.

The time-dependence of the energy transfer rate could be due to one of the following processes:

1) Single-step electric dipole-dipole interaction between randomly distributed sensitizers and activators,

2) Multi-step energy migration on a one-dimensional lattice, and

3) Trap-modulated energy migration in three-dimensional lattice.

Energy transfer by single-step electric dipole-dipole interaction can be verified by theoretical prediction for the energy transfer given by the expression (5)

$$\omega_{sa} = \frac{4}{3} \pi^{3/2} C_a R_o^3 (\tau_s t)^{-1/2} \qquad \text{(V-11)}$$

where C_a is the activator concentration, τ_s is the intrinsic fluorescence decay time of sensitizer, and R_o is the critical interaction distance

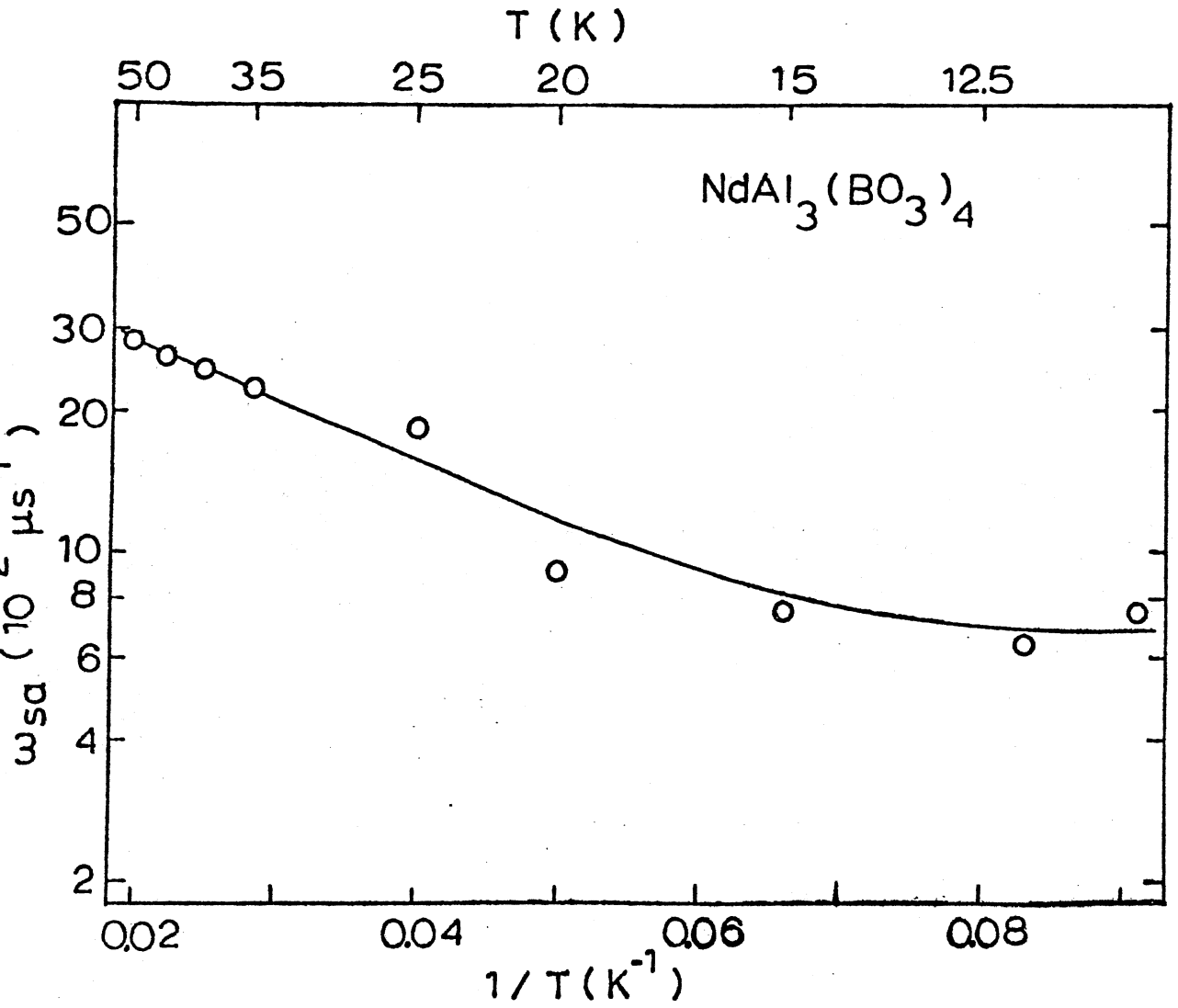

Figure 22. Temperature Dependence of the Energy Transfer Rate Between Nd^{3+} Ions in $NdAl_3(BO_3)_4$. (See Text for Explanation of the Theoretical Line)

TABLE XI

TEMPERATURE DEPENDENT INTEGRATED FLUORESCENCE INTENSITY RATIOS AT A TIME AFTER THE LASER PULSE OF 5919Å FOR $NdAl_3(BO_3)_4$ AND ENERGY TRANSFER RATES DETERMINED

T(K)	$\frac{t = 1\ \mu s}{I_{8827}/I_{8820}}$	$\omega_{sa}\ (\mu s^{-1})$ $\left(\frac{n_a^{(o)}}{n_s^{(o)}} = 1.1,\ k''' = 0.21\right)$
11	0.303	7.56×10^{-2}
12	0.288	6.1×10^{-2}
15	0.301	7.4×10^{-2}
20	0.316	8.8×10^{-2}
25	0.424	18.2×10^{-2}
30	0.440	21.2×10^{-2}
35	0.468	21.5×10^{-2}
40	0.497	23.6×10^{-2}
45	0.516	24.9×10^{-2}
50	0.567	28.3×10^{-2}

given by (17,18)

$$R_o = \left[\frac{3}{4}\left(\frac{e^2}{mc^2}\right) f_a \frac{\Omega\, \phi_s\, \phi_a}{(2\pi\eta\tilde{\nu}_{sa})^4}\right]^{1/6} \qquad \text{(V-12)}$$

where ϕ is the quantum efficiency of the $^4F_{3/2}(a)$ to $^4I_{9/2}(1)$ transition and assumed to be equal for both types of ions, η is the index of refraction of material, $\tilde{\nu}_{sa}$ is the average wavenumber in the region of spectral overlap, f_a is the oscillator strength which for the Lorenzian spectral line shapes can be approximated as (45)

$$f_a = \frac{mc}{\pi e^2} \int \sigma(\nu)\, d\nu \approx \frac{mc}{8\pi^2 e^2 \tilde{\nu}_a^2 \tau_s} \qquad \text{(V-13)}$$

where the ratio of statistical weights for transitions from sensitizer and activator sites being assumed to be normalized to unity. f_a is found to be 2.3×10^{-4}. Ω is the spectral overlap integral which is approximated by the overlap of two Lorentzian lines as

$$\Omega \approx \frac{1}{\pi} \frac{\Delta\tilde{\nu}_s + \Delta\tilde{\nu}_a}{(\Delta\tilde{\nu}_s + \Delta\tilde{\nu}_a)^2 + (\tilde{\nu}_s^o - \tilde{\nu}_a^o)^2} \qquad \text{(V-14)}$$

and is found to be 0.016 cm for this case.

Using the measured value of ω_{sa} in Equation (V-11) along with the values of $C_a \approx 1.4 \times 10^{21}$ cm^{-3} determined by comparing the relative spectral intensities for sensitizers and activators under different pumping conditions and $\tau_s \approx 50$ μs measured in lightly doped samples (37) gives a measured value of $R_o \approx 3\text{Å}$. At 11K, the theoretically predicted value of R_o, using Equations (V-12) and (V-13) along with the value of

$\phi \approx 0.40$, was found to be about 7.8Å which is significantly different from the measured value.

The inconsistent results described above lead us to examine the second type of energy transfer involving an exciton random walk on a one-dimensional lattice. The Nd^{3+} ion in the excited metastable state is treated as a Frenkel exciton which can migrate among sensitizers before getting trapped at an activator site. In this case, the rate of energy transfer can be expressed as the rate at which the exciton samples new sites multiplied by the fraction (N_a) of the total sites occupied by activators and is given by (37)

$$\omega_{sa} = (2/\pi)^{\frac{1}{2}} N_a [\tau_s^{-1} (R_o/R)^6]^{\frac{1}{2}} t^{-\frac{1}{2}} \qquad \text{(V-15)}$$

with the assumption that each step in the random walk takes place through an electric dipole-dipole interaction mechanism between ions separated by R which was taken to be 5.91Å, the closest Nd^{3+} ion-ion separation in this system. Using this value along with the measured value of ω_{sa} in Equation (V-15) gave a value of $R_o \approx 7.2$Å which is consistent with the theoretically predicted value.

Attempts were made to fit the data with two- and three-dimensional random walk models and also with single-step higher order multipole processes, but no good fit was obtained. The most reasonable fit thus was found to be the one-dimensional random walk theory. To explain the temperature dependence Equation (V-15) as a sum over all the thermally activated transitions involved in the exciton migration. In this case, the sum was simplified by taking only two terms into account for the ground state and its first excited component and the energy transfer rate was thus expressed as

$$\omega_{sa} = \left(\frac{2}{\pi}\right)^{\frac{1}{2}} N_a \left\{ \left[t_{H1}^{-1} \frac{1}{1 + e^{-\Delta E_{12}/kT}} \right]^{\frac{1}{2}} + \left[t_{H2}^{-1} \frac{e^{-\Delta E_{12}/kT}}{1 + e^{-\Delta E_{12}/kT}} \right]^{\frac{1}{2}} \right\} t^{-\frac{1}{2}} \qquad \text{(V-16)}$$

where t_{H1} and t_{H2} are the hopping times involving the two types of transitions. The good theoretical fit to the data as shown by the solid line in Figure 22, was found with $\Delta E_{12} \approx 60\ cm^{-1}$, $t_{H1}^{-1} \approx 0.075\ \mu s^{-1}$ and $t_{H2}^{-1} \approx 6.75\ \mu s^{-1}$. Both the value of activation energy and the fact that $t_{H2}^{-1} > t_{H1}^{-1}$ are consistent with spectral observation (33). The room temperature spectrum shows that the "a-1" transitions is more intense then "b-1" so that energy transfer should not increase as b level becomes populated from level a, but transitions to level 2 are more intense implying stronger absorption transitions when this level is populated. The value of $t_{H1}^{-1} \approx 0.075\ \mu s^{-1}$ is consistent with the theoretical prediction of $t_{H1}^{-1} = \tau_s^{-1} \left(\frac{R_o}{R}\right)^6$. The diffusion coefficient at low temperatures is found to be $D = \frac{1}{2} (R^2/t_{H1}) \approx 1.3 \times 10^{-10}\ cm^2\ sec^{-1}$.

Discussions on Results of $Nd\ Al_3(BO_3)_4$

The significant difference between the observed value for R_o and its theoretical estimate clearly indicates that the energy transfer by single-step electric dipole-dipole interaction is not possible in this particular system.

Since any type of trap distribution necessary to obtain a good fit to the data can be postulated, the energy transfer process by trap-modulated energy migration in three-dimensional lattice can not simply

be discarded. The fundamental question here is whether or not exciton motion restricted to one-dimension is feasible in this system. According to recent structural measurements (35), the NAB crystals have a two-dimensional layered structure. Nevertheless, more study on the feasibility of exciton motion in a preferred direction is necessary to have better understanding about the exciton transfer mechanism.

CHAPTER VI

PHOTOACOUSTIC SPECTROSCOPY OF Nd^{3+} IONS IN $YVO_4:Nd^{3+}$ CRYSTALS

Two types of photoacoustic spectroscopy experiments were performed on yttrium vanadate crystals doped with 2% and 3% neodymium impurity ions. First, the variations of PA signal intensities with the chopping frequency of the incident light were measured and then the determination of the quantum efficiencies of the samples were made.

Experimental Results and Discussions

The PA signals at maximum phase were recorded at different chopping frequencies ν_c from 105 Hz to 2000 Hz after the excitation with the 5145Å line of the argon ion laser the power of which was continuously monitored and stabilized at a level of 0.15 W. The results are shown on Figure 23 and tabulated in Table XII for 2% and 3% Nd^{3+} doped samples. For both the samples, the PA signal varies as ν_c^{-1} throughout the entire range of chopping frequencies.

Understanding the above mentioned results became a problem in terms of the present theories on PA signal generation. Three parameters are necessary for theoretical analysis: the sample thickness ℓ, the optical penetration depth ℓ_{op}, and the thermal diffusion length ℓ_{th}. The sample thicknesses were between 1 and 3 mm. The optical penetration depth, characterized by $1/\alpha$ where α is the absorption coefficient at the exci-

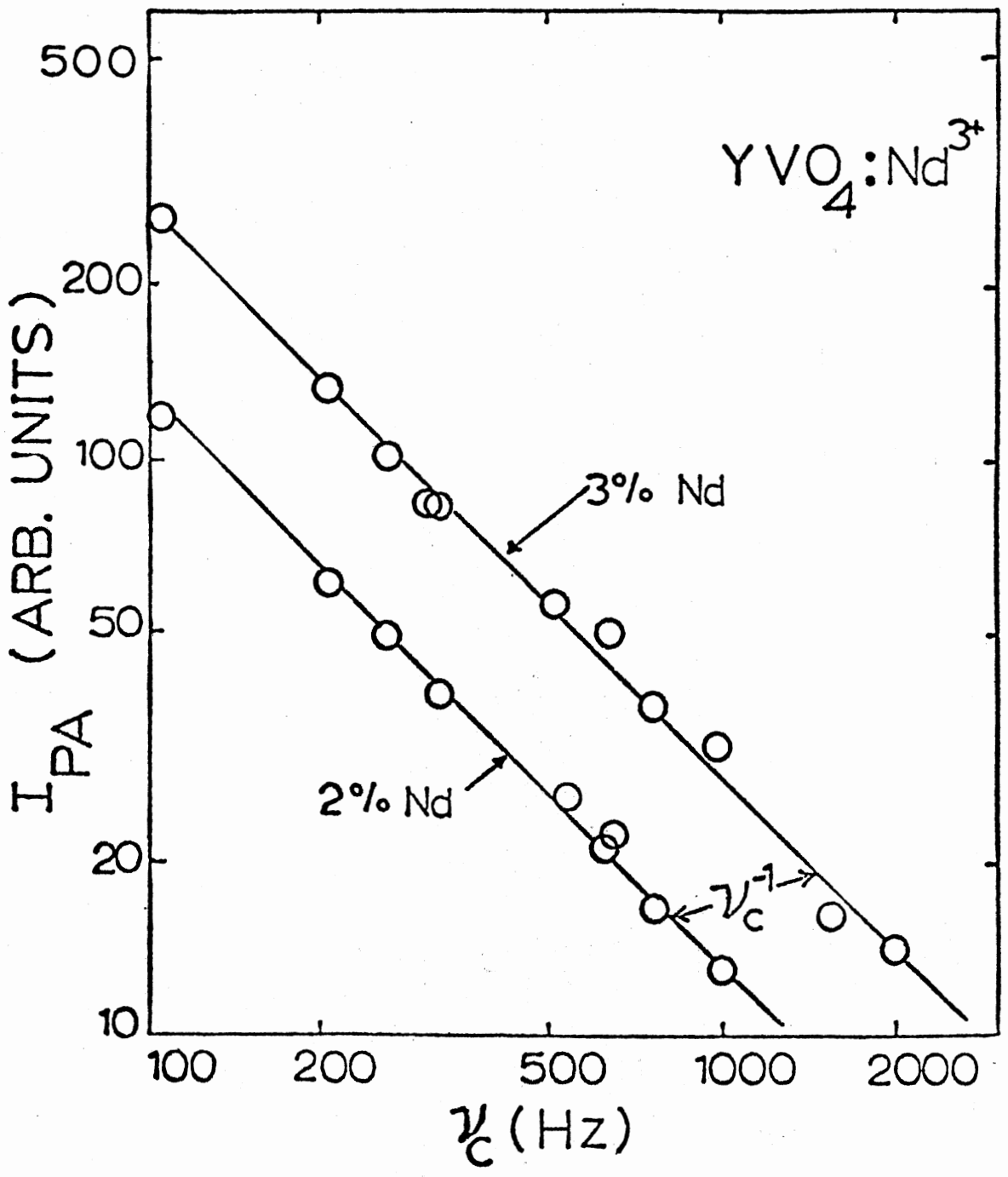

Figure 23. Photoacoustic Signal Intensity as a Function of Chopping Frequencies for Nd-Doped YVO_4 Crystals

TABLE XII

PA SIGNAL INTENSITY AT DIFFERENT CHOPPING FREQUENCIES

ν_c (Hz)	$YVO_4:Nd^{3+}$ (2%) I (arb. units)	$YVO_4:Nd^{3+}$ (3%) I (arb. units)
105	1.170	2.64
208	0.610	1.35
263	0.530	1.04
323	0.425	0.84
526	0.260	0.57
645	0.25	0.50
770	0.164	0.37
1000	0.130	0.32
1540	0.100	0.16
2000	0.098	0.14

tation wavelength, was found to be about 0.7 mm for the samples. It was, therefore, an "optically opaque" case (38). The thermal diffusion length is defined by $\ell_{th} = \sqrt{\beta/(\pi\nu_c)}$, where β is the thermal diffusivity. For yttrium vanadate the thermal diffusivity is about (22) 1.0×10^{-2} cm^2 sec^{-1}. Therefore, for both the samples $\ell_{th} << \ell$, which is the "thermally thick" case (38). Of course, in both samples, $\ell_{th} < \ell_{op}$.

According to the Rosenwaig-Gersho (RG) theory (38), for thermally thick case, the PA signal intensity should vary as $\nu_c^{-3/2}$ which is significantly different from what was observed as shown in Figure 23. The possible reason for this discrepancy between theory and experiment is that the RG theory is based on a one-dimensional model where the thermal gradient at the boundary between the excited surface and the gas causes an uniform heat flow inside the PA cell. According to our experimental set-up, only a small area of the whole sample surface was excited by the very narrow laser beam and the heat was generated in a cylindrical volume within the crystal. Near the surface, a temperature gradient exists between the sample and the gas and the heat generated in that region diffuses to the surface and contributed to the PA signal according to the one-dimensional model. But the temperature gradient inside the sample is radially outward from the heated cylinder. Most of the heat there will not reach the surface and thus will not contribute to the signal. Under these situations, only a smaller layer of thickness ℓ_{eff} near the surface of the sample is effective in the PA signal generation and that takes the place of ℓ_{op} in the RG theoretical assumption. However, the experimental data shown in Figure 23 was in agreement with the recent theory of three-dimensional photoacoustic effect with solids developed by Chow (43).

Determination of Quantum Efficiencies

The maximum PA signal intensity and the phase at which signal intensity was maximized were recorded for two excitation wavelengths of 4765Å and 5147Å at two chopping frequencies of 312 and 1000 Hz as listed in Table XIII.

The signal intensity maximized at the phase θ can be expressed by (44)

$$I_a(\theta) = C(P_a/E_a) \sum_{i,j} \phi_{ij}^{nr} E_{ij} \cos[\psi + \tan^{-1}(2\pi\nu_c\tau_i) - \theta] \qquad \text{(VI-1)}$$

where C is factor accounting for the properties of the PA cell and detection systems, P_a and E_a are the power absorbed and the energy of a certain level "a" where absorption occurs, ϕ_{ij}^{nr} is the probability for a nonradiative transition between levels i and j separated by the energy E_{ij} and τ_i is the lifetime of the initial state i, and ψ is the phase shift due to the detection process. The summation is taken over all the relaxation processes that occur after absorption and can be evaluated by considering the energy level scheme and transitions for Nd^{3+} as shown in Figure 24. For the argon laser lines used as the source of excitation, the absorption occurs in either the $^4G_{11/2}$ or $^2G_{9/2}$ levels at energies E_7 or E_6 respectively. Immediately after the absorption the excited states relax through the cascad of nonradiative decay processes to the $^4F_{3/2}$ metastable state from which radiative decay can occur with a rate W_R to the various ^4I_J multiplets of the ground state with branching ratios b_{5i}. The metastable state can relax also through nonradiative processes with a rate W_{NR}, or through cross-relaxation with neighboring Nd^{3+} ions. This process is commonly known as concentration quenching

TABLE XIII

DATA FOR QUANTUM EFFICIENCY DETERMINATION

ν_c (Hz)	$YVO_4:Nd^{3+}$ (2%)			$YVO_4:Nd^{3+}$ (3%)		
	I_a (arb. units)	I_b (arb. units)	I_b/I_a	I_a (arb. units)	I_b (arb. units)	I_b/I_a
312	0.209	0.480	2.297	0.322	0.744	2.31
1000	0.125	0.288	2.304	0.149	0.334	2.24

λ_a = 4765Å

λ_b = 5145Å

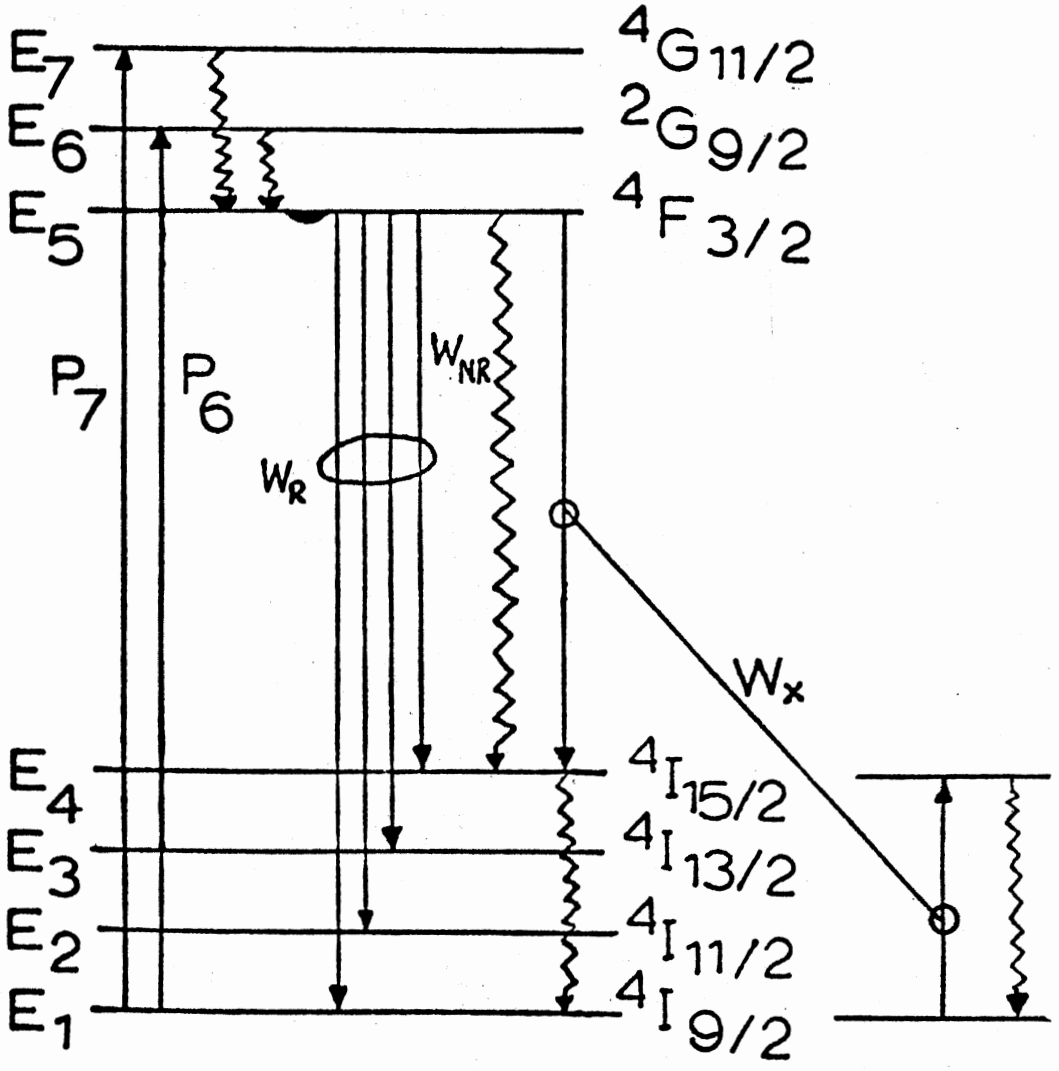

Figure 24. Schematic Diagram of Energy Levels and Transitions for Nd^{3+} Ions

and occurs at the rate of W_x. The quantum efficiency, probability of nonradiative decay, and probability of concentration quenching of the metastable state are given by

$$QE = W_R/T$$

$$P_{NR} = W_{NR}/T \qquad \text{(VI-2)}$$

$$P_x = W_x/T$$

where $T = W_R + W_{NR} + W_x$, and $QE + P_{NR} + P_x = 1$ (VI-3)

The energy levels, branching ratios (24) and lifetimes for the Nd^{3+} ions in both the samples are known. Since only level $^4F_{3/2}$ has a long enough lifetime to cause a phase shift in PA signal, with the help of the model of Figure 24 the signal intensity of Equation (VI-1) can be reexpressed as

$$I_a(\theta) = C(P_a/E_{a1})[E_{a5}\cos(\psi-\theta) + (E_{51}-kQE) \times \cos\{\psi + \tan^{-1}(2\pi\nu_c\tau_5)-\theta\}] \qquad \text{(VI-4)}$$

where

$$k = E_{51} - b_{54}E_{41} - b_{53}E_{31} - b_{52}E_{21},$$

and

τ_5 is the lifetime of the level $^4F_{3/2}$.

To eliminate the factor C which is not possible to determine, the ratio of PA signal intensities at two different excitation wavelengths were taken and the solution for quantum efficiency is given by

$$QE = \frac{A\left[E_{75}\cos(\psi-\theta_7) + E_{51}\cos\{\psi + \tan^{-1}(2\pi\nu_c\tau_5) - \theta_7\}\right] \\ -E_{65}\cos(\psi-\theta_6) - E_{51}\cos\{\psi + \tan^{-1}(2\pi\nu_c\tau_5) - \theta_6\}}{k\left[A\cos\{\psi + \tan^{-1}(2\pi\nu_c\tau_5)-\theta_7\} - \cos\{\psi + \tan^{-1}(2\pi\nu_c\tau_5) - \theta_6\}\right.} \quad \text{(VI-5)}$$

where,

$$A = (I_6/I_7)(E_{61}/E_{71})(P_7/P_6) \quad \text{(VI-6)}$$

The phase shift due to the long relaxation of the metastable state was another problem to determine and because of additional contributions to the phase shift due to the electronic equipment eventually this was solved by taking the derivative of Equation (VI-4) with respect to the phase angle θ and equating it to zero for the maximization of signal intensity; solving for another expression for quantum efficiency gives

$$QE_a = \frac{1}{k}\left[\frac{E_a\sin(\psi-\theta_a)}{\sin\{\psi + \tan^{-1}(2\pi\nu_c\tau_5) - \theta_a\}} + E_{51}\right] \quad \text{(VI-7)}$$

A pair of similar expressions (VI-7) for two different excitation wavelengths along with the Equation (VI-5) can be solved itteratively to obtain a unique value for quantum efficiency. The calculated values for QE are tabulated in Table XIV and compared with values obtained from other measurements. The uniqueness of the PAS results for QE was checked by repeating the entire calculation at both low and high chopping frequencies.

Inspite of many problems the PAS technique gave results consistent with other measurements. The calculation of QE was very sensitive to the parameter A given by (VI-6). The ratio of signal intensities could

TABLE XIV

QUANTUM EFFICIENCIES

Sample	QE	
	PAS Method	Other Method
$YVO_4:Nd^{3+}$ (2%)	0.59	0.53[a]
$YVO_4:Nd^{3+}$ (3%)	0.54	0.51[b]

(a) From lifetime measurements and radiative lifetime (24).

(b) From lifetime quenching measurements (40).

be measured accurately and the ratio of the energies of the excitation lines was also known exactly, but the ratio of the power absorbed at the two excitation wavelengths was difficult to determine accurately. Another problem was measuring the amount of light scattered at the cell window and the sample surfaces as well as in determining the exact absorption coefficients for the sharp absorption line at the positions of very narrow laser lines. However, PAS is a very powerful technique to obtain information on radiationless relaxation processes of ions in solids and can successfully be used to determine quantum efficiencies even in complicated cases involving numerous radiationless processes, provided enough information concerning energy levels and branching ratios are available. Since absolute measurements are difficult it is, therefore, important to develop better experimental methods of eliminating cell and measuring system response characteristics, and it is important to further develop theoretical models to account for different types of experimental conditions as well.

CHAPTER VII

SUMMARY AND CONCLUSIONS

The host-sensitized energy transfer in yttrium vanadate single crystals doped with trivalent neodymium impurity ions was found to be consistent with a single-step electric dipole-dipole interaction process at low temperatures where the excitons are self-trapped, whereas at high temperatures the energy transfer became dominated by thermally activated excitons hopping among other host molecular ions accompanied by trapping process at activator. Some similar investigations (18,19) previously conducted on the same host doped with different types of trivalent rare earth impurities were found to be consistent with the model proposed to interpret the exciton transfer process in our samples. Though this experiment itself is fairly simple to conduct significant information regarding exciton transfer from host to impurity ions can be obtained.

Laser time-resolved site-selection spectroscopic studies were conducted on two types of single crystals: yttrium vanadate doped with neodymium ions and neodymium aluminum borate (NAB) crystals. The results obtained for the first type of crystals were found to be consistent with a multi-step diffusion type of energy transfer with the mechanisms for diffusion and trapping both involving a two-phonon-assisted process proposed by Holstein et al. (29). In the case of neodymium aluminum borate crystals, on the other hand, the energy trans-

fer characteristics were consistent with a one-dimensional random walk with a phonon-assisted hopping process. These characteristics in NAB are very different from those found in other neodymium doped crystals (30,32,40). These differences could possibly arise from the complicated structure of NAB crystals which is not yet completely worked out (35).

Previous site-selection spectroscopy studies on yttrium vanadate host crystals doped with trivalent europium impurity ions (19) showed that the energy transfer results were consistent with a single-step resonant electric dipole-dipole interaction process. This difference in energy transfer characteristics for different impurity ions could be due to much higher concentration of neodymium ions in yttrium vanadate crystals.

It was, however, found that a reasonable fit was obtained by computer simulation only with an exceedingly large value of critical interaction distance. The reason for this discrepancy is not precisely known at the present moment. It is hoped that the modification of the computer simulation technique will eliminate the discrepancy in near future.

The problem of energy transfer by migration among non-uniformly distributed impurity ions in a solid was analytically attacked by Burshtein (11,12). The main difference between this case and the normal diffusion one where the impurity ions are considered to be uniformly distributed, is that the hopping time of exciton varies in each step in random walk depending on the local environment of activators. Though the Burshtein's approach is quite simple and straightforward it involves many approximations of which the most severe one is the assumption of a constant and average hopping time, which obviously eliminates the

importance of the random-walk problem. Since there is no better theoretical technique available to handle this problem, at present a Monte-Carlo computer simulation technique (14) was used to interpret our TRS data.

However, because of immense potential of these materials as laser host, the investigation of them with the same host doped with different impurity ions and using higher resolution dye laser will be reasonable continuation of this research work in order to obtain better understanding of the important and fundamental physical processes underlying their optical properties.

Finally, laser photoacoustic spectroscopy measurements were performed on neodymium ions in vanadate crystals. The results of the frequency dependence of the PA signals were not in agreement with the predictions of one-dimensional theoretical model (38). However, our results were in agreement with the recently developed (43) three-dimensional model for PA signal generation. The quantum efficiencies measured by the PAS technique were in good agreement with the results obtained by other predictions or measurements. Important feature about PAS technique is that enough information on radiationless relaxation processes of ions in solids can be achieved with this simple technique. There are still some difficulties for absolute measurements of quantum efficiencies, which, can be eliminated to some extent by improving cell-system response properties.

BIBLIOGRAPHY

1. Förster, T., Ann. Physik 2, 55 (1948); Z. Naturforsch 49, 321 (1949).

2. Dexter, D. L., J. Chem. Phys. 21, 836 (1953).

3. Frenkel, J., Physik. Z. Soujet Union 9, 158 (1936).

4. Yokota, M. and O. Tanimoto, J. Phys. Soc. Japan 22, 779 (1967).

5. Eisenthal, K. B. and S. Siegel, J. Chem. Phys. 41, 652 (1964).

6. Inokuti, M. and F. Hirayama, J. Chem. Phys. 43, 1978 (1965).

7. Trlifaj, M., Czech. J. Phys. 5, 463 (1955).

8. Merkle, L., Ph.D. dissertation, OSU (1978).

9. Gennel, P. G., J. Phys. Chem. Solids 7, 345 (1958).

10. Chandrasekhar, S., Rev. Mod. Phys. 15, 1 (1943).

11. Burshtein, A. I., Soviet Phys. JETP 35, 5 (1972).

12. Burshtein, A. I., Soviet Phys. JETP 22, 4 (1966).

13. Watts, R. K., in Optical Properties of Ions in Solids.

14. Chow, H. C. and R. C. Powell, Phys. Rev. B21 (1980).

15. Karpman, V. I., Non-linear Waves in Dispersive Media, pp. 33, Pergamon Press, Oxford, New York (1975).

16. Morse, P. M. and H. Feshbach, Methods of Theoretical Physics, Volume I (pp. 972, McGraw-Hill, New York, 1953).

17. Johnson, L. F., Optical Maser Characteristics of Rare-Earth Ions in Crystals, J. Appl. Phys. 34, 4 (1963), pp. 897-907.

18. Hsu, C. and R. C. Powell, J. Lum. 10, 273 (1975); G. E. Venikouas and R. C. Powell, J. Lum. 16, 29 (1978).

19. Venikouas, G. E. and R. C. Powell, Phys. Rev. B 17, 3456 (1978).

20. Levine, A. K. and F. C. Palilla, Appl. Phys. Lett. 5, 118 (1964).

21. O'Conner, J. R., Appl. Phys. Lett. 9, 407 (1966).

22. Rubin, J. J. and L. G. VanVitert, J. Appl. Phys. 37, 2970 (1966).

23. Yaney, P. P. and L. G. DeShazer, J. Opt. Soc. Am. 66, 1405 (1976).

24. Lomheim, T. S. and L. G. DeShazer, J. Appl. Phys. 49, 5517 (1978).

25. Hong, H. Y-P., and K. Dwight, Mat. Res. Bull. 9, 1661 (1974).

26. Bilak, V. I. et al., Sov. Phys. 240, 585 (1978).

27. Venikouas, G., Ph.D. Dissertation, May, 1978, Oklahoma State University.

28. Soos, Z. G. and R. C. Powell, Phys. Rev. B 6, 4035 (1972).

29. Holstein, T., S. K. Lyo, and R. Orbach, Phys. Rev. Lett. 36, 891 (1976).

30. Merkle, L. D. and R. C. Powell, Phys. Rev. B 20, 75 (1979).

31. Kushida, T., J. Phys. Soc. Japan 34, 1381 (1973); 34, 1327 (1973); 34, 1334 (1973).

32. Zokai, M., R. C. Powell, G. R. Imbush, and B. DiBartolo, J. Appl. Phys. 50, 5930 (1979).

33. Chinn, S. R. and H. Y-P Hong, Optics Comm. 15, 345 (1975).

34. Powell, R. C. and Z. G. Soos, Phys. Rev. B5, 1547 (1972).

35. Danielmeyer, H. G., presented at the International Laser Symposium, 1979.

36. Weber, M. J., Phys. Rev. B4, 2932 (1971).

37. Chinn, S. R. and W. K. Zwicker, J. Appl. Phys. 49, 5892 (1978).

38. Rosenwaig, A. and A. Gersho, J. Appl. Phys. 47, 64 (1976).

39. Lomheim, T. S. and L. G. DeShazer, Optics Comm. 24, 89 (1978).

40. Flaherty, J. M. and R. C. Powell, Phys. Rev. B 19, 36 (1979).

41. Watts, R. K., J. Opt. Soc. Am. 61, 123 (1971).

42. Montroll, E. W., Proc. Symp. Appl. Math. Am. Math. Soc. 16, 193 (1963).

43. Chow, H. C., J. Appl. Phys. (in press).

44. Merkle, L. D. and R. C. Powell, Chem. Phys. Letters 46, 303 (1977).

45. DiBartolo, B., Optical Interaction in Solids (John Wiley, New York, New York, 1968).

VITA

Dhiraj Kumar Sardar

Candidate for the Degree of

Doctor of Philosophy

Thesis: LASER SPECTROSCOPY STUDIES OF $YVO_4:Nd^{3+}$ AND $NdAl_3(BO_3)_4$ CRYSTALS

Major Field: Physics

Biographical:

Personal Data: Born in Merudandi of Basirhat Sub-Division, 24 Parganas, West Bengal, India, October 10, 1948, son of Harekrishna and Dasibala Sardar.

Education: Graduated from Basirhat High School, West Bengal, India, July, 1965; received Bachelor of Science degree from University of Calcutta, Calcutta, India, in 1968; received Master of Science degree from University of Calcutta, Calcutta, India, in 1970; completed requirements for the Doctor of Philosophy degree in July, 1980.

Professional Experiences: Lecturer in Physics, Ramakrishna Mission Residential College Affiliated to University of Calcutta, India, 1971-72; Lecturer in Physics, Basirhat College under University of Calcutta, India, 1972-1975; Graduate Teaching Associate, Department of Physics, Oklahoma State University, 1976-1978; Graduate Research Associate, Department of Physics, Oklahoma State University, 1979-1980.